NASA Technical Memorandum 88364

USAAVSCOM Technical Memorandum 86-A-6

A Comparison of the Acoustic and Aerodynamic Measurements of a Model Rotor Tested in Two Anechoic Wind Tunnels

D.A. Boxwell, F.H. Schmitz, W.R. Splettstoesser and K.J. Schultz, S. Lewy and M. Caplot

(NASA-TM-88364) A COMPARISON OF THE ACOUSTIC AND AERODYNAMIC MEASUREMENTS OF A MODEL ROTOR TESTED IN TWO ANECHOIC WIND TUNNELS (NASA) 56 p CSCL 01A

N87-15178

Unclas
G3/02 40323

November 1986

National Aeronautics and Space Administration

United States Army Aviation Systems Command

NASA Technical Memorandum 88364 USAAVSCOM Technical Memorandum 86-A-6

A Comparison of the Acoustic and Aerodynamic Measurements of a Model Rotor Tested in Two Anechoic Wind Tunnels

D. A. Boxwell, Aeroflightdynamics Directorate, US Army Aviation Research and Technology Activity, Ames Research Center, Moffett Field, CA
F. H. Schmitz, Ames Research Center, Moffett Field, CA
W. R. Splettstoesser,
K. J. Schultz, DFVLR, Braunschweig, Federal Republic of Germany
S. Lewy,
M. Caplot, ONERA, Chatillion, France

November 1986

National Aeronautics and Space Administration
Ames Research Center
Moffett Field, California 94035

United States Army Aviation Systems Command
St. Louis, Missouri 63120

A COMPARISON OF THE ACOUSTIC AND AERODYNAMIC MEASUREMENTS OF A MODEL ROTOR TESTED IN TWO ANECHOIC WIND TUNNELS

D. A. Boxwell
Aeroflightdynamics Directorate
U.S. Army Aviation Research and Technology Activity (AVSCOM)
Moffett Field, California, U.S.A.

F. H. Schmitz
NASA Ames Research Center
Moffett Field, California, U.S.A.

W. R. Splettstoesser and K. J. Schultz
DFVLR
Braunschweig, Federal Republic of Germany

S. Lewy and M. Caplot
ONERA
Chatillion, France

ABSTRACT

Two aeroacoustic facilities--the CEPRA 19 in France and the DNW in The Netherlands--are compared. The two facilities have unique acoustic characteristics that make them appropriate for acoustic testing of model-scale helicopter rotors. An identical pressure-instrumented model-scale rotor was tested in each facility and acoustic test results are compared with full-scale-rotor test results. Blade surface pressures measured in both tunnels were used to correlate nominal rotor operating conditions in each tunnel, and also used to assess the steadiness of the rotor in each tunnel's flow. In-the-flow rotor acoustic signatures at moderate forward speeds (35-50 m/sec) are presented for each facility and discussed in relation to the differences in tunnel geometries and aeroacoustic characteristics. Both reports are presented in appendices to this paper.

1. INTRODUCTION

Model-rotor aeroacoustic testing in wind tunnels by industry and government research organizations in both the United States and Europe is now commonplace (refs. 1-4). The impetus for this testing includes the recently imposed commercial noise regulations for terminal-area operation of helicopters, the ever-increasing use of wind tunnels by rotorcraft companies, and the use of new materials that allow the fabrication of accurately scaled rotor models. It is becoming increasingly important that manufacturers assess the acoustic characteristics of proposed new designs early in the development process. If the newly designed or modified rotorcraft is too noisy, it may not meet the requirements for flight in commercial airspace. Model-scale acoustic testing is proving to be an effective means of making that assessment.

There are two levels of aeroacoustic testing--one for parametric design changes and one for quantification of fundamental noise-generation processes. There have been many successful attempts to assess the potential design changes on the radiated noise field. Full-scale acoustic data taken in the 40- by 80-ft wind tunnel at Ames

This paper was given at the 12th European Rotorcraft Forum, Sept. 1986, Garmisch-Partenkirchen, Federal Republic of Germany

Research Center in the early 1970s demonstrated the benefits of thin tips for high-speed helicopter flight. Model-scale data have also shown the effects of tip shape on the blade-vortex interaction noise of rotorcraft (ref. 4). In all of these experiments, the fidelity of the parametric results depended on the aerodynamic and acoustic properties of the testing facility and the degree to which the rotor testing was representative of full-scale flight. Wind tunnels with little reverberation in the frequency range of interest generally provide higher-quality acoustic results than those that are overly reverberant. Similarly, those rotors with properly scaled aerodynamic and dynamic characteristics captured the important aerodynamic and acoustic phenomena and yielded more quantitative results. In most of this parametric testing, it was hoped that the phenomena under consideration were accurately represented so that the effect of parametric design changes on the radiated noise of the actual helicopter rotor would be correct.

More quantitative aeroacoustic testing of model-scale rotors has been shown for certain types of helicopter noise. An in-flight, far-field method was used to gather a high-quality, full-scale acoustic data base that was free of ground reflections (ref. 5). The resulting data were used to compare the results of wind-tunnel tests of aerodynamically similar models. When correct nondimensional parameters were held constant, excellent scaling of high-speed impulsive noise was demonstrated. Good scaling at low advance ratios for blade-vortex interaction noise was also shown. In neither case was it necessary to make corrections for Doppler shifts, ambient temperature, and wind effects. The phenomena of interest were quantitatively scaled.

Although always desirable, in many instances testing of this kind may not always be feasible. As a consequence, an important and interesting question arises: How much do the aerodynamic and acoustic properties of the facility itself influence the model-scale results? This paper addresses this question by comparing two different anechoic wind tunnels: the CEPRA 19 in France and the DNW in The Netherlands.

The test rotor was identical and the test itself was operated in an identical manner in the two tunnels. The rotor was instrumented with many surface-pressure transducers to define as completely as possible the aerodynamics of the blade. An assessment of the aerodynamic and acoustic properties of both facilities is presented here. This is followed by a comparison of selected acoustic signatures and blade pressures under similar flight conditions. A comparison is made with full-scale results.

2. FACILITY CHARACTERISTICS: GENERAL FEATURES

Testing of the rotor model was first conducted in an anechoic wind tunnel located in France at CEPr (Center for Propulsive Studies) near Paris. This facility CEPRA 19 is of the open-circuit, open-test-section design and is one of the largest open-circuit anechoic wind tunnels in the world (fig. 1a). A concrete test chamber, which surrounds the open jet, is about one quadrant of a sphere with a 9-m radius. The walls and floor are lined with acoustic wedges that are 1 m long, giving an acoustic cutoff frequency of about 200 Hz. Both the entrance and diffuser portions of the tunnel circuit are anechoically treated with acoustic baffles to protect the test chamber from exterior and tunnel-drive-system background noises.

The free jet is 12 m long. A circular 3-m-diam nozzle was installed for these tests; theoretically it allows a maximum jet velocity of 60 m/sec. The resulting flow is collected by a large, solid fiberglass collector and extracted by a centrifugal pump to the outside through the acoustic baffling system. For these tests, both the nozzle and collector were made of hard-surface fiberglass, and the nozzle lip was treated with 10 cm of serrated acoustic foam. An adjacent control room housed all measurement instrumentation and wind-tunnel and rotor drive controls. Table 1 lists the major geometric and flow characteristics of the free jet. It should be noted that the level of transverse turbulence (1.1%) for CEPRA 19 in Table 1 is equivalent to rms angle of attack variations of at least 0.6° in the jet. More detailed information about the CEPRA 19 facility is given in appendix A where it is also indicated that modifications at the CEPRA 19 facility since these tests were run have improved the flow quality by an order of magnitude.

The DNW is a closed-return-type, subsonic atmospheric wind tunnel with three interchangeable, closed-test-section configurations and one open-jet aeroacoustic configuration; the latter was used for the model rotor tests. Figure 1b shows the arrangement of the various components of the DNW.

The open-jet configuration consists of a 6- by 8-m nozzle with a testing hall surrounding the open jet that is 45 m long, 30 m wide, and 20 m high. The testing hall walls are acoustically treated and provide good anechoic properties. The open-jet configuration was designed to obtain low background noise levels at flows up to 80 m/sec. This was accomplished by choosing a low-tip-speed fan (blade-tip Mach number of 0.5) and by acoustically lining the turning vanes and the inner collector and transition walls. The major geometric and flow characteristics of the free jet are also summarized in table 1 for comparison with the CEPRA 19 data. The comparative transverse turbulence level in the DNW of <0.1% (rms angle-of-attack variation of about 0.1°) indicates that the jet flow is quite steady at frequencies above 0.2 Hz. More detailed information about the DNW facility characteristics that are relevant to rotor aeroacoustic testing is given in appendix B.

3. ROTOR INSTALLATION CHARACTERISTICS

The rotor used in both tests was a 1/7-scale model of the AH-1/OLS full-scale, pressure-instrumented blades used for aerodynamic and noise testing by NASA. The model rotor was instrumented with a number of miniature pressure transducers to measure local surface-pressure distributions on the rotor blades. A more complete description of the rotor test stand is provided in reference 2 for the CEPRA 19 entry and in reference 3 for the DNW test. Figures 2a and 2b, taken from these references, illustrate the rotor installation in the open jet of each facility. For each installation, a number of microphones were distributed around the rotor--both within the free jet and outside of the open-jet core flow.

Inherent in wind-tunnel testing of model helicopter rotors is a large variety of possible operating conditions, one of which is the variation of the rotor's tip-path-plane angle with respect to the free flow. For both tunnels, the rotor installation assumed that the airflow qualities of the open jets would not be influenced by the test stand and would be as given in appendices A and B. Open-jet wall corrections were

estimated before testing, but were not used to alter the planned test conditions. Instead, parametric sweeps were conducted in both tunnels in order to carefully map out critical testing parameters; for instance a sweep of the rotor tip-path-plane angle, which was known to be sensitive to any open jet boundary effects. In this manner, blade-vortex interaction (BVI) geometries critical to rotor acoustics would not be missed in either tunnel installation. (The effect of this will be seen in data presented in a later section).

The acoustic characteristics of each facility, however, were not assumed to be those of previously published tunnel surveys (summarized in appendices A and B). The effect of rotor installation (e.g., struts and fairings) on each tunnel's acoustic environment was investigated before testing was begun. Two methods were used: (1) background tunnel noise measurements (no rotor running) and (2) impulsive calibrations.

Background Noise

Background noise was measured on all microphones--both in the flow and out of the flow for both tunnels. Results are presented for inflow microphone locations in the rotor plane and at 30° below the rotor-tip-path plane at a distance 1.5 diam from the rotor hub. One objective of this paper is to make a direct comparison of the model-scale acoustics of each tunnel with full-scale in-flight results. The effect of open-jet shear layer flow on radiated acoustics is beyond the scope of this work.

Background noise measurements were analyzed from dc to 10 kHz with no high-pass filtering. A narrow-band analysis of 40-Hz resolution was chosen so that broadband spectrum levels would be the same as the planned analysis of the rotor acoustic signature. Standard ensemble averaging was used.

The measured levels for the in-plane microphone as a function of tunnel velocity, are illustrated in figure 3a for CEPRA 19 and in figure 3b for the DNW.

The inflow noise levels for both tunnels are characterized by higher spectrum levels at frequencies below 100 Hz and by a gradual decay in level toward the higher frequencies, where levels are typically dominated by wind-induced noise from the nose cone on the microphone. Above 35 m/sec, the CEPRA 19 spectra show generally higher noise levels above 100 Hz. Part of this increase in level occurs around discrete frequencies, probably a result of vortex shedding from microphone struts or other pieces of the rotor installation structure. The CEPRA 19 background noise at 50 m/sec exhibits a gradual increase in level with frequency that is thought to result from broadband loads on the microphone nose cone and support strut. These loads are likely induced by the larger unsteady angle-of-attack variations in the CEPRA 19 flow, and raise the background threshold by 10 dB at frequencies above 5 kHz. The insert in each of the figures shows more clearly the low-frequency background noise spectrum levels near the rotor fundamental blade-passage frequency of 80 Hz. Here the background levels are nearly the same order of magnitude as the expected rotor noise levels, but averaging techniques can be used to remove this effect from the lower rotor-noise harmonics.

Background noise for the inflow microphone located 30° below the rotor plane is shown in figures 4a and 4b for CEPRA 19 and DNW, respectively. The evidence of shedding noise in CEPRA 19 has diminished at this location, and DNW levels at 80 m/sec have increased slightly, probably a result of shear-layer proximity.

IMPULSE CALIBRATIONS

In the second method for assessing the anechoic properties of each of the two tunnels, impulses (small explosive charges mounted in the plane of the rotor disk and fired electrically) were used to determine acoustic reflections. The initial reflection tests revealed unwanted acoustic reflections from the 3-m nozzle lip in CEPRA 19 and from the microphone support struts in the DNW. These areas were covered with acoustically absorptive material for the purpose of reducing reflections by at least 10 dB.

Figures 5 and 6 show the time-histories of the reflection tests for each facility for the two microphone positions considered in these comparisons. The time-histories for the in-plane microphones (figs. 5a-5d) in both tunnels indicated that the reflections were significantly reduced, with the DNW almost approximating free-field conditions. Unfortunately, and because of scaling constraints, the CEPRA 19 microphone located 30° below the rotor plane (figs. 6a, 6b) was positioned close to the 3-m nozzle structure and exhibited a measured reflection that was stronger than desired. The problem became more intense with flow in which multiple nozzle and/or shear-layer reflections were observed to follow the initial impulse. The effect of these reflections is to distort both the time-histories and the power spectra of the measured rotor noise.

4. ROTOR ACOUSTIC COMPARISONS

Figures 7-9 present a direct comparison of the model-scale OLS blade acoustic signature measured in each of the two facilities and the comparable full-scale 540-rotor signature measured in-flight. The a, b, and c parts of figures 7-9 illustrate the time-history over one revolution; parts d, e, and f show the corresponding power spectra. The time-histories are presented in both instantaneous and averaged form. The model-scale time-histories begin, conventionally at the downstream blade position, whereas for the full-scale results, the starting reference for the revolution is arbitrary. Two types of power spectra are presented, the first of which is the average power spectrum; the second is a single power spectrum of the averaged time-history. Both power spectra are displayed over a harmonic frequency axis where each line unit is a measure of rotor rotational rate (about 40 Hz for model scale). For this two-bladed rotor, every other line in the spectrum is exactly a rotor harmonic of blade-passage frequency. The 250-line frequency responses in these figures therefore correspond to about 10 kHz in model scale.

Figure 7 presents acoustic comparisons for an in-plane microphone at a nominal advance ratio of 0.164. As will be explained in the following section, blade pressures were used to determine comparable rotor flight conditions in each facility. Figure 7a presents CEPRA 19 data at a rotor-tip-path-plane angle of 3.5°; figure 7b presents DNW data at 1°, indicating a 2.5° jet angularity difference between facilities at this

rotor advance ratio and thrust coefficient. The full-scale results in figure 7c were measured during a 400 ft/min rate of descent. The time-histories show good overall similarity between model-scale results, especially when an order of magnitude difference in unsteady inflow angles exists between facilities. The average DNW time-histories are, however, more distinct than those in CEPRA 19. The comparable full-scale signature levels are low, possibly because of slight inaccuracies in the directivity angle for the in-plane micropnone. The frequency-domain results follow these same trends with the DNW spectra having a better signal-to-noise ratio than CEPRA 19. The differences in low-frequency spectral shapes are probably because the CEPRA 19 in-plane microphone is located within the hardwall nozzle, while differences at higher frequencies are thought to be related to the larger angle-of-attack variations of CEPRA 19. These effects would make the quantitative description of rotor impulsive noise more difficult. It should be noted that the average power spectrum retains the tail-rotor-related frequencies in the full-scale measurements, whereas the power spectrum of the average time-history has successfully removed them. This allows a more direct comparison of model- and full-scale results.

Figure 8 illustrates the same flight condition, at the microphone position 30° below the rotor plane. At this measurement location, the BVI acoustic signature is stronger in both model- and full-scale results; however, the CEPRA 19 data show the effect of tunnel-nozzle contamination, mentioned earlier in the discussion of impulse calibrations. The rotor signature near the CEPRA 19 nozzle depicts a wider thickness noise component, probably owing to nozzle or shear-layer reflections. This is also indicated by the higher level, low-frequency content in the CEPRA 19 spectral plots. Similar higher frequency spectral differences between the two facilities are also noted at this 30° down microphone position. The DNW data are again more distinct than the CEPRA 19 data and scale with the full-scale data quite well.

Figure 9 presents results for the in-plane microphone at an advance ratio of 0.224. For this higher advance ratio, a tip-path-plane correction of 2° between model-scale facilities was determined. Differences between model-scale and full-scale peak pressure levels and waveforms of the BVI signature become more evident at this higher speed. The CEPRA 19 data are the least well defined, but neither model-scale test closely replicates the full-scale results. Differences in actual measurement angles and unsteady flow angularities are two possible explanations. The power spectra also indicate this deterioration. In the CEPRA 19 tunnel, the signal-to-noise ratio of the acoustic signature is generally lower and the spectral shapes are different when compared with DNW data for the reasons cited earlier. The DNW power spectra are better defined but exhibit a marked difference when compared with full-scale data. No known reason for these discrepancies has been identified.

5. ROTOR AERODYNAMIC COMPARISONS

The 1/7 geometrically scaled AH-1/OLS model rotor tested in both CEPRA 19 and the DNW was instrumented with 50 miniature pressure transducers: 32 absolute, flush-mounted Kulite transducers on one of the blades and 18 differential pressure transducers on the second blade. The absolute transducer locations were chosen to match some of the radial and chordwise transducer positions in the full-scale NASA

Operational Loads Survey tests. The geometrical characteristics of the model blades and model-scale transducer locations are given in reference 6.

One flight condition at an advance ratio of 0.164 was chosen for illustrating the comparison of blade pressure measurements in each facility. For this advance ratio and at constant thrust coefficient, a parametric sweep of tip-path-plane angle was completed in each facility. This rotor angle sweep (from -5° to +7° in the DNW and from 0° to +5° in CEPRA 19) placed the rotor in a series of flight conditions (descents) known to produce blade-vortex interactions. The measured blade loads during this parametric sweep of rotor tip-path-plane angle were extensively analyzed and compared for each facility. This procedure clearly showed an angular tip-path-plane correction between facilities of about 2.5° at an advance ratio of 0.164. (A simple theoretical wall correction model used in reference 3 indicated that a 1.5° correction was appropriate to match CEPRA 19 model data with full-scale data.) The 2.5° correction was used in the following comparisons and also shows that the blade pressures are a much more sensitive indicator of incidence corrections between facilities than relying on the similarity in acoustic signatures.

Figure 10 presents averaged upper-surface, leading-edge (3% chord) blade-pressure time-histories at four blade radial stations. Figures 10a and 10b show the CEPRA 19 and DNW results, respectively. Correlation is generally very good on an average basis. For the most part, the higher unsteadiness levels of the CEPRA 19 tunnel (when these data were acquired) can be successfully removed from the blade-pressure measurements by signal processing. However, there are some notable differences in the sharpness of the advancing blade-vortex interaction pulse as seen in figure 10. The higher transverse turbulence levels of the CEPRA 19 tunnel could have smoothed the blade-vortex pressure time-history. There are also some differences at the downstream blade position, probably owing to wake effects from the rotor strut; that is, the rotor in the CEPRA 19 tunnel is flapped back about 2.5° more with respect to the rotor strut fairing than it is in the DNW. This effect is more pronounced for the tip transducers than for inboard transducers.

Figure 11 compares the upper- and lower-surface leading-edge (3% chord) blade pressures at nearly the same radial station (within 1% of 96% blade radius). Figures 11a and 11b show good overall correlation for both instantaneous and averaged time-histories. The instantaneous signal was chosen to be comparable to the averaged signal level over the sampling period. The DNW blade surface pressure data near the advancing blade-vortex interaction locations are sharper than the same data taken in the CEPRA 19 tunnel. This results in a slower harmonic falloff in the power spectrum of the DNW data when compared with the CEPRA 19 data. This effect is shown in figures 11c and 11d. These power spectra are computed on two-revolution time-histories. This gives a frequency resolution and reponse (250 lines) of about 20 Hz and 5 kHz, respectively. The slightly slower harmonic decay with increasing harmonic number is evident in the DNW data, suggesting that a more impulsive event was measured in the DNW blade pressure data. This also is consistent with the observation that the measured acoustic data are more impulsive in the DNW wind tunnel.

6. CONCLUSIONS

Both the CEPRA 19 and DNW facilities exhibit in-the-flow background noise levels low enough to permit the accurate measurement of model-rotor radiated impulsive acoustic signatures. In the DNW, the rotor impulsive noise signature was above in-flow background noise levels at flow velocities up to 80 m/sec. For CEPRA 19, the background noise levels were slightly higher than the DNW, probably due to the higher turbulence levels. Some pseudo-tonal noise (above 5 kHz) was evident in the CEPRA 19 background noise during this test and therefore also in the rotor acoustic signature at tunnel velocities between 35 and 50 m/sec.

For the size of the rotor that was tested (2-m diam), the DNW in its 6- by 8-m open jet nozzle configuration allowed placement of in-flow microphones farther from the nozzle structure and from the free-jet shear layer than in the CEPRA 19 with its 3-m nozzle. Impulsive calibrations indicated that the 3-m nozzle of the CEPRA 19 would contaminate the microphone data at the 30° below the rotor-plane position where strong BVI impulsive noise signatures are radiated. These effects were observed in the CEPRA 19 data in both the time and frequency domains.

Acoustic waveforms, for the in-plane microphone measurements, ahead of the rotor, were similar for both facilities. Some differences in the level of the high-speed thickness noise were observed. These differences may be attributed to the reverberation characteristics of the CEPRA 19 nozzle (the in-plane microphone was just inside the nozzle) or to the sensitivity of high-speed thickness noise levels to near in-plane microphone positions. Because of the small, but different, jet-flow angles in these two facilities, the "in-plane" microphones probably were not actually in the rotor's tip-path plane.

Higher rms transverse turbulence levels (an order of magnitude) in CEPRA 19, as compared with the DNW, also affected the measured acoustic data. Although the spectral shape in the lower frequency harmonics (100 to 2,000 Hz) was generally the same in both facilities, differences in specific harmonic levels of up to 10 dB were noted. In addition, the CEPRA 19 acoustic harmonics became less discrete at lower frequencies than in the DNW acoustic spectra.

Blade-pressure measurements taken during rotor-tip-path-plane parametric sweeps indicated that a 2.5° tip-path-plane angular flow difference (wall correction effect) existed between the two facilities at an advance ratio at 0.164 and thrust coefficient of 0.0054. This was in contrast to a theoretically estimated value of 1.5°. When the experimental correction was accounted for, averaged measured blade pressures were very similar in character in both facilities. Dynamic blade pressure time-histories caused by advancing blade-vortex interactions, were more distinct in the DNW than in CEPRA 19. This also was evident by the slower roll-off of the blade-pressure harmonics measured in the DNW and can probably be attributed to the lower turbulence levels in the DNW tunnel.

In summary, both the CEPRA 19 and the DNW wind tunnels are useful for rotorcraft aeroacoustic testing. The recent modifications to the CEPRA 19 tunnel should improve the quality of measured rotor blade pressures and, hence, the radiated rotor noise in future tests, hopefully

bringing CEPRA 19 measurements to a level comparable with the DNW. Because the jet size in the DNW is roughly twice that in CEPRA 19, it is possible, in the DNW, to take in-flow measurements farther into the acoustic far-field, for the same size rotor, with minimum contamination from tunnel constraints. However, this same size differential makes the accomplishment of these measurements much more difficult.

APPENDIX A
CEPRA 19 ANECHOIC WIND TUNNEL

S. Lewy and M. Caplot
(with O. Papirnyk and J. C. Bohl)

This appendix provides only those characteristics of the CEPRA 19 anechoic wind tunnel that are relevant to the main text; that is, the data pertinent to the 3-m nozzle at the time of the rotor tests (beginning of 1981). Note that until now, this configuration of the wind tunnel was used only for rotor tests and is thus less documented than the 2-m-nozzle configuration, which allows flow velocities up to 100 m/sec. It must also be emphasized that some improvements to the facility, already done or planned for the near future, make some of the following numbers obsolete.

AXIAL FLOW DATA

Information on the mean axial component U of the flow velocity is given in figure 12. Figure 12a presents a top view with the definition of the axes (z is oriented downward). The origin of the coordinates is taken at the center of the sphere. With these notations, the location of the rotor hub is

$$x = -2.677 \text{ m}, \quad y = 0, \quad z = -0.445 \text{ m}$$

Figures 12a and 12b are relative to a nominal velocity on the axis of the wind tunnel of $U_o = 50$ m/sec. The use of the 3-m nozzle in these tests was its first, and the speed was limited at about 55 m/sec. It is planned to equip the centrifugal blower of the wind tunnel with a new gearbox in order to achieve a 70 m/sec velocity, a velocity that is of interest for testing a large range of helicopter flight conditions.

The turbulence level of the axial fluctuations at the abscissa of the rotor hub ($x = -2.677$ m, $z = -0.375$ m) are shown in figure 13a for the low-frequency components (rms value in the range 0.125-2.5 Hz) and in figure 13b for the range of 2.5-500 Hz. The power spectral density (PSD) of the axial velocity fluctuations u near the hub ($y = 0.1$ m) is shown in figure 14a and that near the advancing-blade tip location ($y = 0.90$ m) is shown in figure 14b. This point is close to the beginning of the mixing layer of the jet (see fig. 12b). The very-low-frequency part of the spectra, under 2 Hz, is due to mass-flow fluctuations on the suction side of the wind tunnel; the higher-frequency component is related to the natural turbulence and to the mixing layer, as can be seen at $y = -0.90$ m.

TRANSVERSE FLOW DATA

The most useful data for interpreting the acoustic measurements on BVI are the flow angles, mainly those around the advancing-blade tip. Figures 15 and 16 show the fluctuations of pitch angle and yaw angle at the height of the rotor hub ($x = -2.677$ m, $z = -0.445$ m). Figures 15a and 16a give the rms values for the low-frequency components (from 0.05 to 20 Hz), which are the most important, and figures 15b

and 16b give values for components in the range 2.5 to 1,000 Hz. In order to facilitate comparisons with DNW data (appendix B), rough scales of the turbulence levels for the horizontal v and vertical w velocity components are also provided, according to the crude relations

$$\alpha(rd) \simeq w/U_o \quad \text{and} \quad \beta(rd) \simeq v/U_o$$

Figures 17a and 18a give the PSD of α and β from 0.1 to 1,000 Hz at the rotor hub (y = 0); figures 17b and 18b, the PSDs at the advancing-blade tip (y = -1 m). Finally, figure 19 shows the time-signatures of α and β for 10 sec at y = 0 and y = -1 m, for U_o = 40 m/sec. The results for the other velocities are quite similar and are thus not reproduced here. These plots document the stationarity of the fluctuations and their peak-to-peak values.

Some modifications of the stagnation chamber (greater length, honeycomb, and grids) have reduced the flow-angle fluctuations in the central part of the potential core (about on one half of its diameter) by one order of magnitude, with a great increase in the stationarity of the signals. New improvements, already checked, will link the rectangular section of the stagnation chamber to the circular inlet section of the nozzle and will extend the previous result to the whole potential core.

BACKGROUND NOISE

The background noise depends on several conditions. For instance, the background noise is different without anything in the flow or with the strut of the model. The location of the measurement is another important parameter: the microphone may be outside or inside the flow and, in the latter location, it may record reflections from the inner part of the nozzle or from the diffuser if it is located far upstream or downstream. The results are also different with and without windscreens on the microphones, because of reverse flows in some parts of the anechoic chamber.

For a given test condition, the overall sound pressure level (OASPL) follows a U^5 to U^6 law as a function of the flow velocity. As an example, figure 20 shows third-octave spectra measured by a 1/4-in. microphone without a windscreen in the plane x = 0, at a distance of 6 m from the center of the anechoic room; the frequency range extends up to 80 kHz, because of some tests on small-scale models.

A more detailed description of CEPRA 19 is given in reference 7, along with the study of refraction and scattering effects through the shear layer of the jet. Other data on reverse flows in the anechoic chamber and on background noise are documented in reference 8.

APPENDIX B
DNW ANECHOIC WIND TUNNEL

AERODYNAMIC CHARACTERISTICS

The quality of a free-jet stream is characterized by stationary and nonstationary aerodynamic criteria. The stationary flow quality may be judged by considering the axial flow deviations and the flow angularity, as well as the temperature distribution. The spatial distribution in kinetic pressure q (corresponding to the mean flow velocity distribution U) in one cross section was measured by a pitot static probe attached to the sting support mechanism at two velocities, 42 m/sec and 74 m/sec. The results show that at this cross section,--that is, at the rotor-hub center, which lies 7 m downstream of the 6- by 8-m nozzle exit--the potential core height measures about 5 m. This corresponds to an angle of "influence" for the shear layer (i.e., $\Delta q/q \geq 2\%$ or $\Delta U/U \geq 1\%$) of about 4° with respect to the lipline. For the larger part of the core the deviations in q (U) are less than 0.5% (0.25%), but are 1% (0.5%) near the periphery. Figure 21 shows the mean flow velocity profiles U(y) in a horizontal plane at the rotor-hub position as a result of measured ($-2.5\ m < y < +2.5\ m$) and extrapolated ($-3\ m > y > +3\ m$) data, the latter being obtained from velocity measurements in the x-z plane and correlated model wind-tunnel test results. Also shown in figure 21 for reference purposes is the size of the rotor diameter, indicating that the rotor operated well within the potential core of the free jet.

The flow angularity in the vertical plane of symmetry of the DNW free jet is generally very low. The mean angle of incidence and angle of yaw distributions, $\bar{\alpha}(z)$ and $\bar{\beta}(z)$, respectively (figs. 22a, 22b), at the model rotor-hub position ($x = 7\ m$, $y = 0\ m$), indicate a marginal downwash on the tunnel centerline of about 0° to -0.1° and a small sidewash of about 0.25° to the starboard (sliding door) side with a bandwidth of ±0.1° in both cases.

A wind-tunnel model placed in the free jet can change the clean-flow configuration considerably, depending on the blocking effect of the model. To assess this influence on the model-rotor inflow, especially the deviations of the mean flow velocity and the angle of incidence, open-jet wind-tunnel corrections have been calculated using the Heyson method (ref. 9).

The spatial uniformity in temperature was measured in the 6- by 8-m center cross section of the closed test section only. Since the level and pattern of possible nonuniformities are, above all, a function of the upstream flow history, the results are also considered valid for the potential core of the free jet. It was found that after 20 min of steady-state tunnel operation (with the cooler working) the temperature uniformity in the core region, which is of most interest for model tests, is better than ±0.2 K.

The nonstationary flow quality is commonly described in terms of the rms values of the three orthogonal components of the velocity fluctuations in relation to the mean velocity, that is, the longitudinal, the lateral, and the vertical turbulence intensities. A related and important question is how the velocity fluctuations are distributed in

the frequency domain, for this is a measure of the size of the eddies and therefore of the sensitivity of the boundary-layer flow past a model.

The calibration measurements (ref. 10) of the turbulence intensities were performed by means of an X-wire probe attached to the DNW sting support mechanism. The hot-wire anemometer output signals were fed after proper bandpass filtering (0.2 to 10,000 Hz) into an rms voltmeter to find the rms intensities. Frequency spectra were obtained by feeding the unfiltered signals into an FFT spectrum analyzer. The results were stored on digital tape cartridges. Unfortunately, no analog recordings of the data have been made so that no time-histories of the velocity fluctions (flow-angularity fluctuations) are available.

The spatial distributions of the measured longitudinal, lateral, and vertical rms turbulence intensities for a horizontal (lateral) traverse through the free jet are shown in figures 23-25 for a flow velocity of 40 m/sec. For reference, the model rotor diameter is also noted, thus allowing an assessment of the rotor inflow turbulence levels, which can be considered as extremely low for open-jet test sections. The longitudinal velocity fluctuations in the range of the rotor inflow are well below 0.3% of the flow velocity, and the two other components are less than 0.15%. These lateral and vertical rms velocity fluctuations are equivalent to nonstationary fluctuations of the angle of yaw and of incidence, respectively, which are shown as a second scale in figures 24 and 25. For the region of interest they are smaller than 0.1°.

The longitudinal and lateral flow fluctuations increase rapidly as soon as the probe is positioned off-center. This is typical for the shear-layer-generated fluctuations that become obvious in the power spectra of the fluctuations discussed later. The shear layer itself, with its intermittent bypass of vorticity, is reached at $y = \pm 3$ m, which is confirmed by the above-mentioned kinetic pressure measurements. The vertical fluctuations remain relatively constant over a considerable horizontal range.

The effect of the tunnel velocity on the longitudinal and lateral turbulence intensities was measured only on the tunnel centerline (fig. 26). The turbulence intensities do not change noticeably in the velocity range over which the BVI noise tests were performend. Although the upstream history of the turbulence should be about the same as for the closed test section, the levels are considerably higher; this is true in particular of the longitudinal fluctuations, which became greater than the lateral fluctuations. This result can be explained by looking into the power spectral density spectra (fig. 27) of the longitudinal fluctuations (fig. 26). Both spectra (one on the tunnel centerline $y = 0$, fig. 27a; one taken at the rotor advancing-blade tip at $y = -1$ m, fig. 27b) are dominated by a hump at 2.5 Hz corresponding to a Strouhal number of 0.4 based on an equivalent contraction exit diameter. This, exactly, is the peak Strouhal number of the fluctuation spectrum on the jet centerline at the model center as induced by the jet's shear layer. The turbulence from upstream appears in the spectrum only for frequencies above 10 Hz but is irrelevant for the rms value of u (since the level is about 40 dB down). Also, owing to the use of a logarithmic frequency axis, the area under the curve is no longer a measure of the mean square value of the fluctuations. The contribution

below 1 Hz, therefore, appears large but in fact contains little rms energy. The corresponding transversal velocity spectra (figs. 28, 29) show that the shear-layer-induced peaks are much less important. The reason is the higher lateral and also vertical fluctuation level from upstream, which is accompanied by a lower shear-layer-induced level that results from the symmetric motion of the jet. The rising fluctuation levels for very low frequencies seem to be a consequence of an unsteady secondary flow within the testing hall; however, these fluctuations are not relevant for aeroacoustic and aerodynamic measurements.

OUT-OF-FLOW BACKGROUND NOISE CHARACTERISTICS

Outside the open-jet flow, the air velocities in the testing hall are small and no wind-induced noise is present when a foam wind-ball is used. The background one-third-octave noise spectra, measured 12.2 m (about 1.6 equivalent nozzle diameters) from the tunnel centerline, are given in figure 30 for three free-jet velocities. From these spectra it can be seen that the noise concentrates at the lower-frequency range and gradually decreases toward the higher frequencies. A sketch of the DNW open test section is shown in figure 31, with microphone positions noted for the clean-tunnel calibrations.

A more detailed description of the DNW is given in reference 11.

REFERENCES

1. Sternfeld, H., Jr., Schaeffer, E. G. — The Role of Wind Tunnel Models in Helicopter Noise Research. 42nd Annual National Forum of the American Helicopter Society, 1986.

2. Schmitz, F. H., Boxwell, D. A., Lewy, S., Dahan, C. — A Note on the General Scaling of Helicopter Blade-Vortex Interaction Noise. 38th Annual National Forum of the American Helicopter Society, 1982.

3. Splettstoesser, W. R., Schultz, K. J., Boxwell, D. A., Schmitz, F. H. — Helicopter Model Rotor-Blade Vortex Interaction Impulsive Noise: Scalability and Parametric Variations. NASA TM-86007, 1984.

4. Hoad, D. R. — Helicopter Model Scale Results of Blade-Vortex Interaction Noise as Affected by Tip Modification. 36th Annual National Forum of the American Helicopter Society, 1980.

5. Schmitz, F. H., Boxwell, D. A. — In-Flight Far-Field Measurement of Helicopter Impulsive Noise. Journal of the American Helicopter Society, Vol. 21, No. 4, Oct. 1976.

6. Boxwell, D. A., Schmitz, F. H., Splettstoesser, W. R., Schultz, K. J. — Helicopter Rotor High-Speed Impulsive Noise: Measured Acoustics and Blade Pressures. NASA TM-85850, 1983.

7. Bongrand, J., Julienne, A., Perulli, M. — Simulation of the Effects of Forward Velocity on Jet Noise in an Open Circuit Wind Tunnel. Workshop on the Effects of Forward Velocity on Jet Noise, NASA Langley Research Center, 1976 (ONERA Preprint No. 1978-6E).

8. Rebuffet, P., Guedel, A. — Tests on an 8/100-Scale Model for the Definition of the Convergent and Collector of CEPRA 19 (Anechoic Open Jet Wind Tunnel). AIAA Paper 81-1989, Palo Alto, Calif., 1981.

9. Heyson, H. H. — Rapid Estimation of Wind Tunnel Corrections with Application to Wind Tunnel and Model Design. NASA TN D-6416, 1971.

10. Michel, U., Froebel, E. — Velocity Fluctuations in the German-Dutch Wind Tunnel Relevant to Rotor Noise Measurements. DFVLR IB-22216-85/B1, 1985.

11. van Ditschuizen, J. C. A.
Courage, G. D.,
Ross, R.,
Schultz, K.-J.

Acoustic Capabilities of the German-Dutch Wind Tunnel DNW. AIAA Paper 83-0146, Reno, Nev., 1983.

TABLE 1.- MAJOR GEOMETRIC AND FLOW CHARACTERISTICS OF CEPRA 19 AND DNW

	CEPRA 19	DNW
Nozzle cross section	Circular; 3-m diam	6 × 8 m
Free jet length, m	11.84	20
Mean flow velocity range, m/sec	0-55	0-85
Axial turbulence level (on centerline at 40 m/sec), %	0.5	<0.3
Transverse turbulence level (on centerline at 40 m/sec), %	1.1	<0.1
$\Delta\alpha$ Peak-to-peak value, deg	3	NA

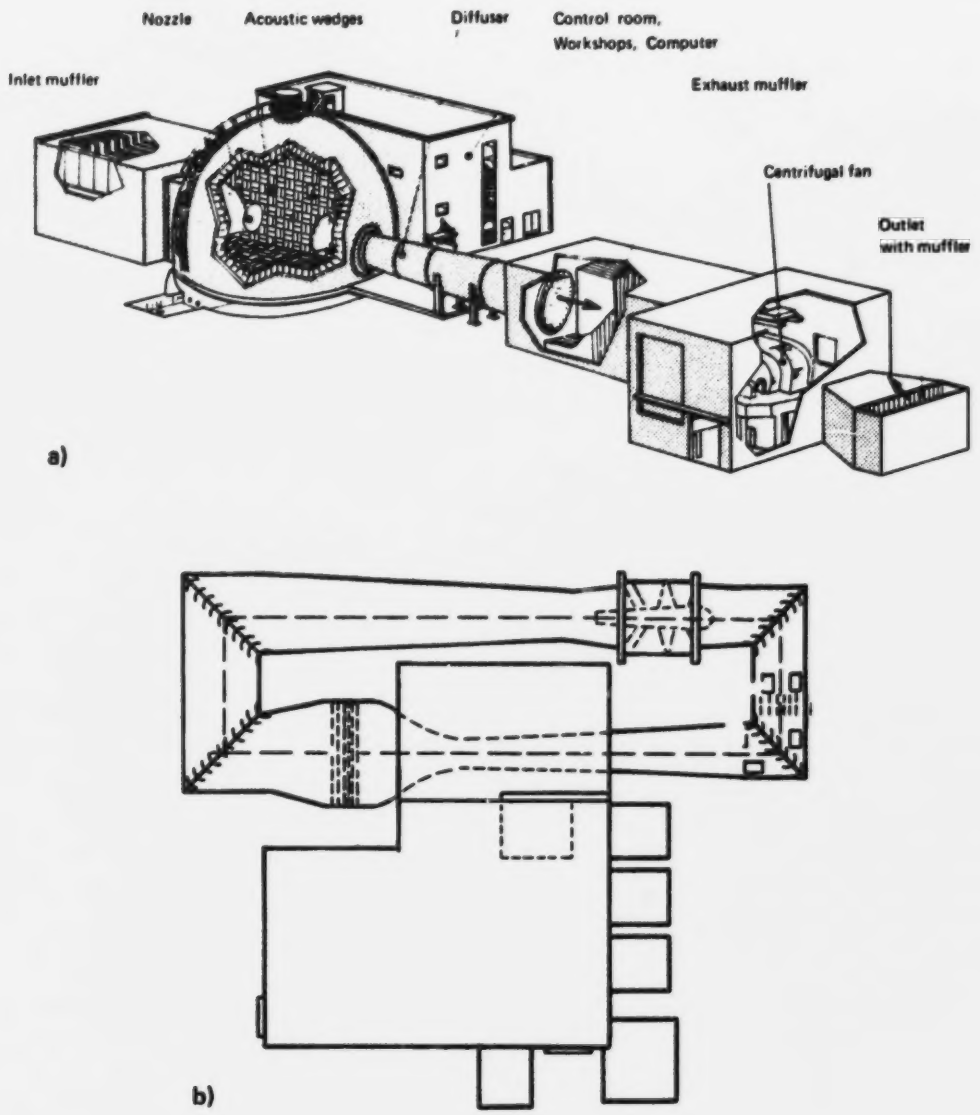

Figure 1.- Anechoic wind tunnels. (a) The CEPRA 19 tunnel; (b) the DNW complex.

ORIGINAL PAGE IS
OF POOR QUALITY

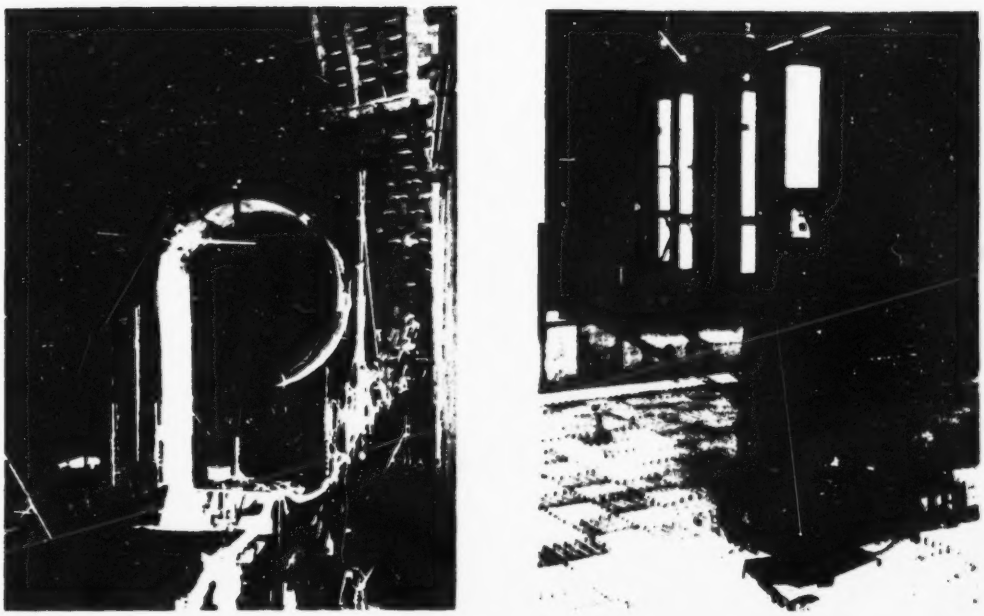

a) b)

Figure 2.- One-seventh-scale model OLS rotor and test stand. (a) Rotor installed in CEPRA 19 anechoic wind tunnel (from ref. 2); (b) rotor test stand mounted in the DNW open test section (from ref. 3).

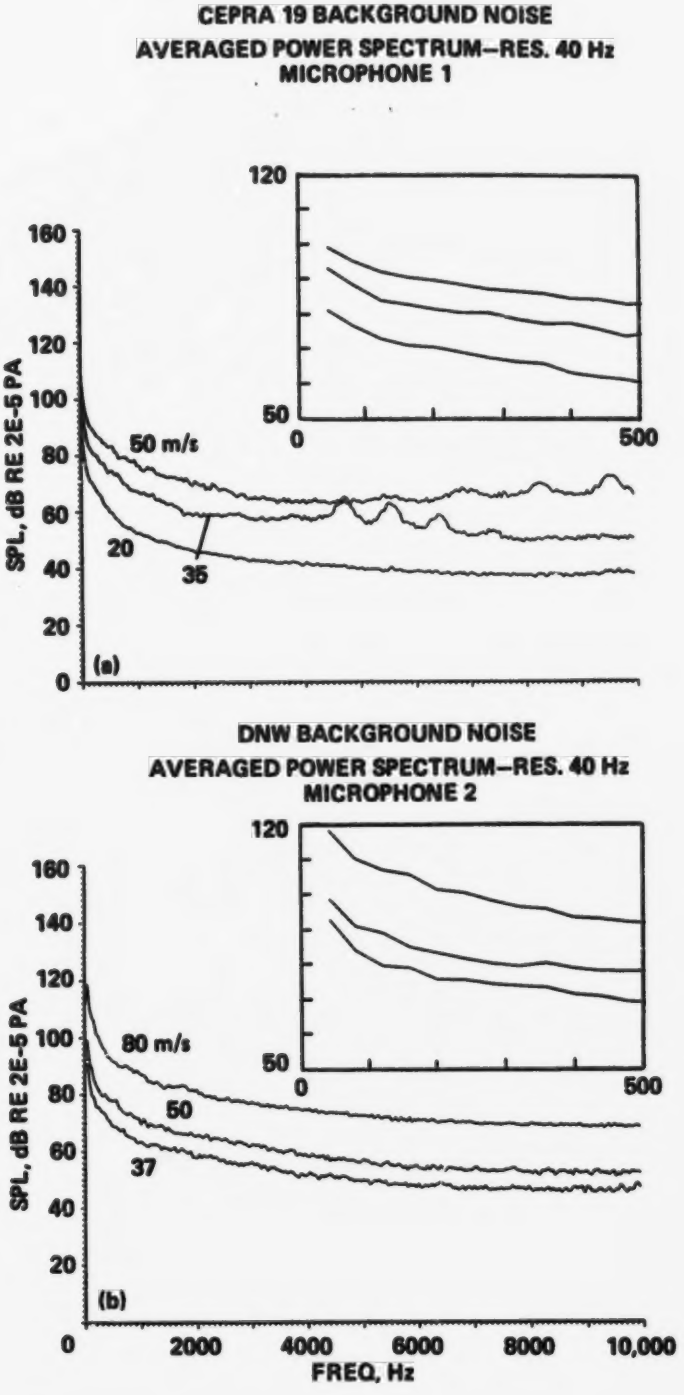

Figure 3.- Background noise versus tunnel velocity: in-plane microphone. (a) CEPRA 19; (b) DNW.

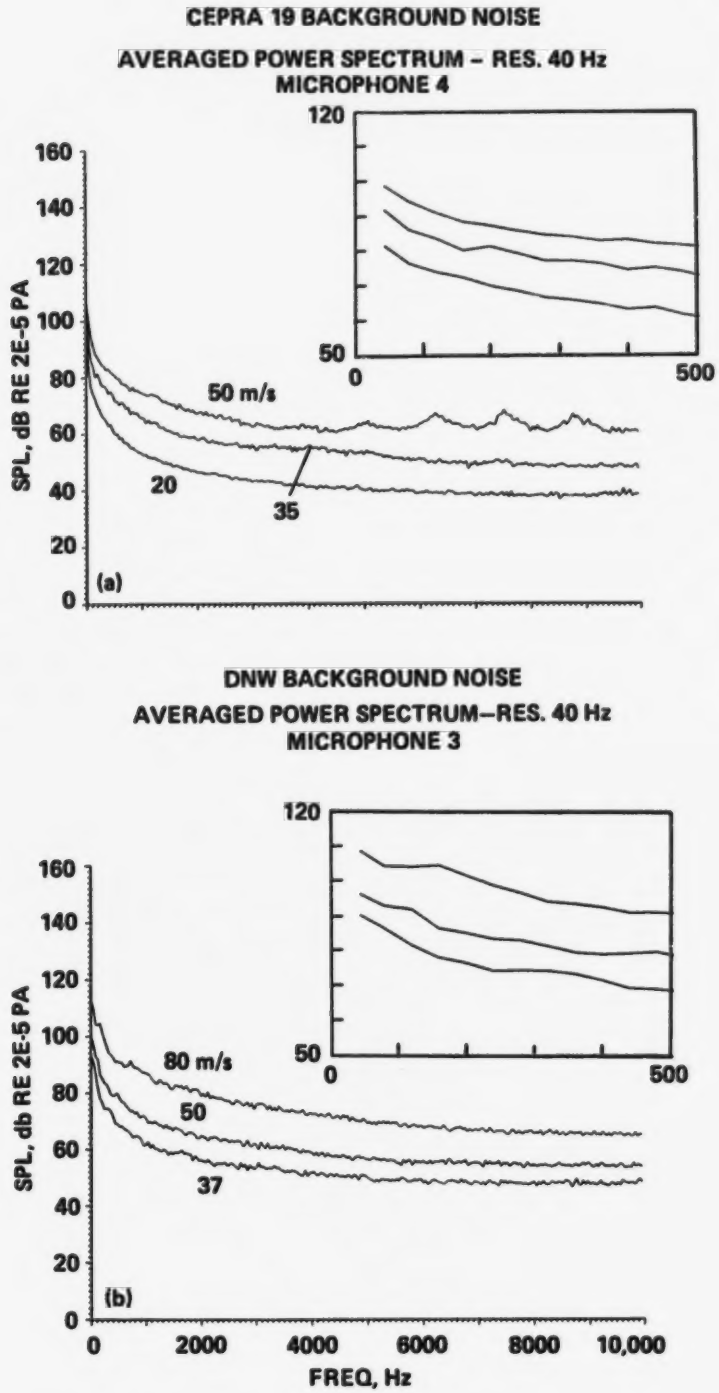

Figure 4.- Background noise versus tunnel velocity: 30° below rotor plane microphone. (a) CEPRA 19; (b) DNW.

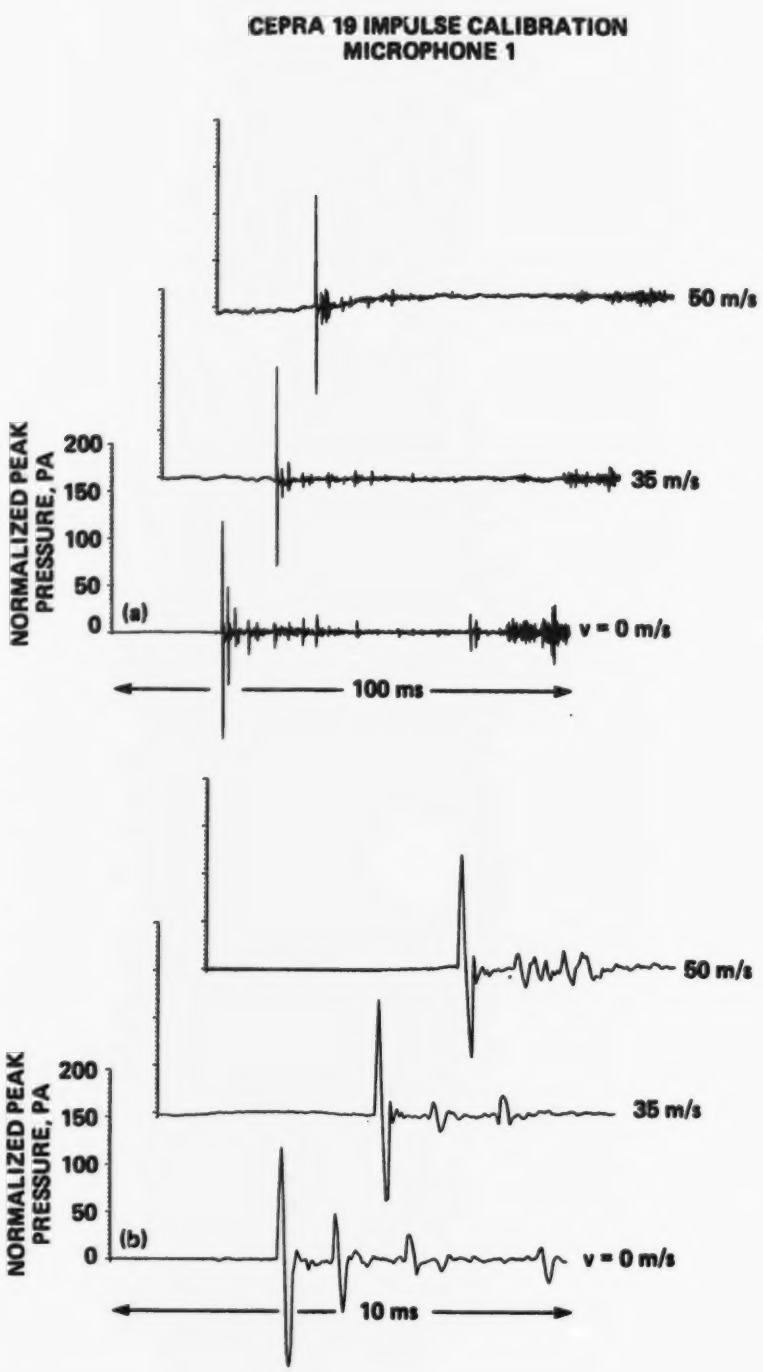

Figure 5.- Wind-tunnel impulse calibration versus tunnel velocity: in-plane microphone. (a) CEPRA 19, 100 msec; (b) CEPRA 19, 10 msec.

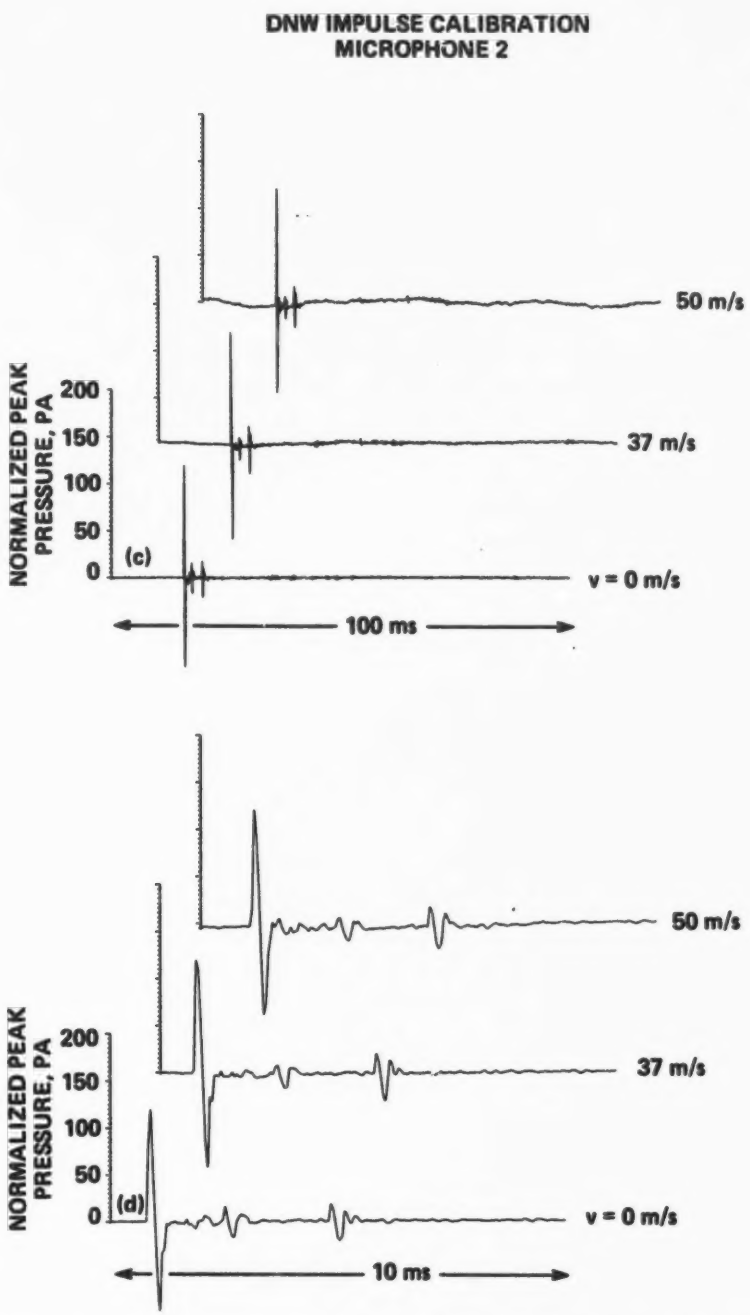

Figure 5.- Concluded. (c) DNW, 100 msec; (d) DNW, 10 msec.

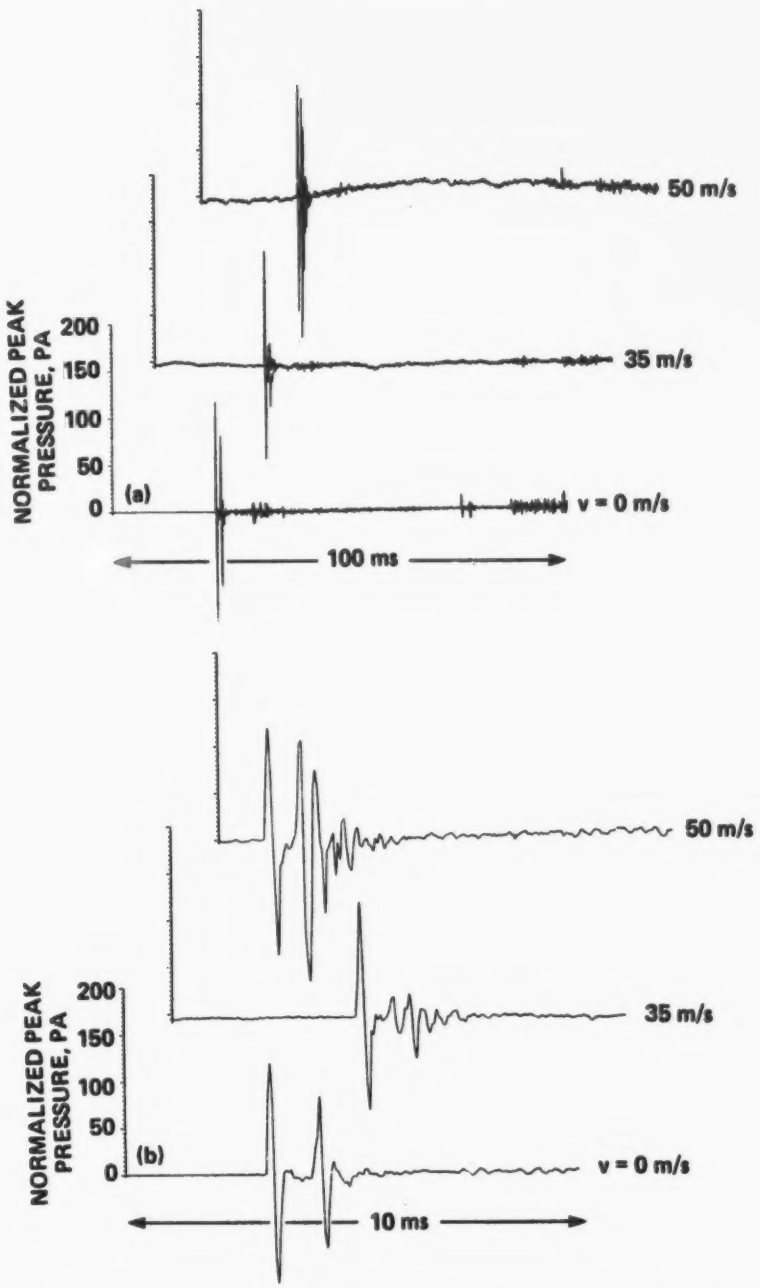

Figure 6.- Wind-tunnel impulse calibrations versus tunnel velocity: 30° below rotor-plane microphone. (a) CEPRA 19, 100 msec; (b) CEPRA 19, 10 msec.

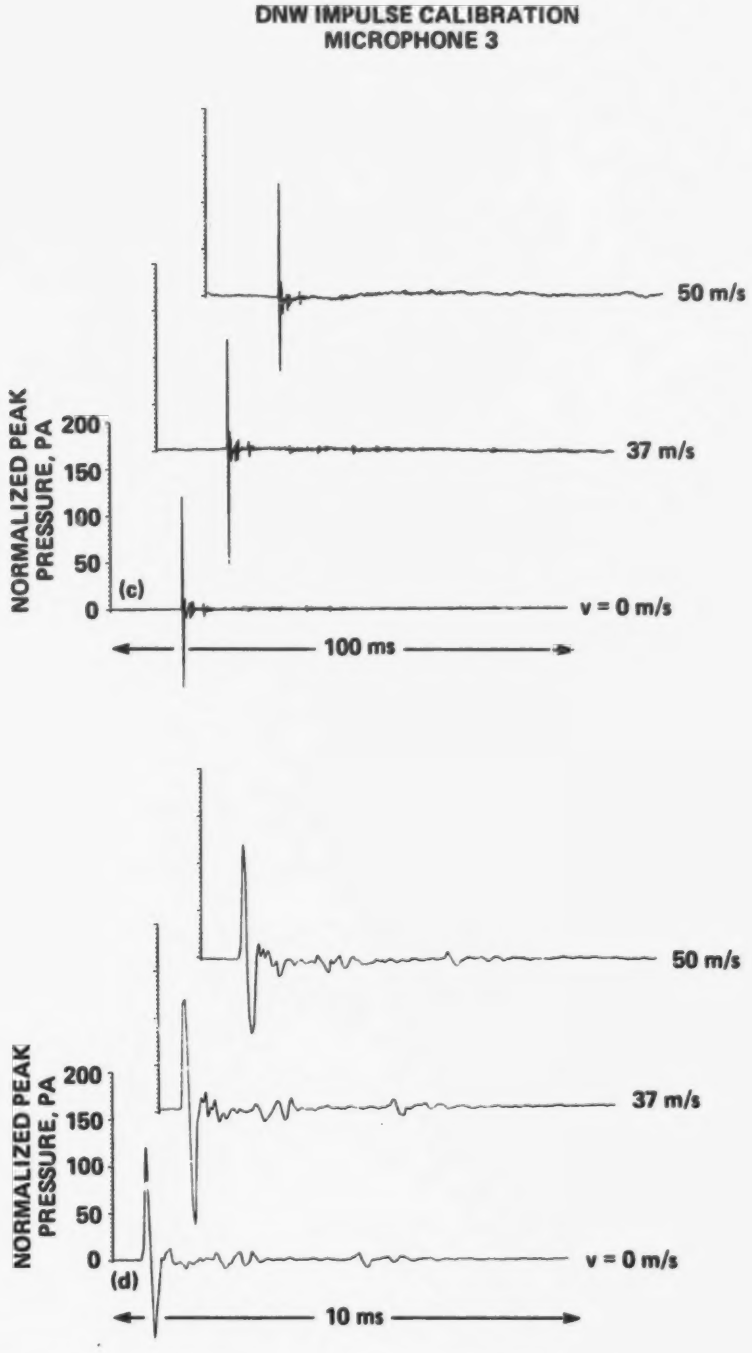

Figure 6.- Concluded. (c) DNW, 100 msec; (d) DNW, 10 msec.

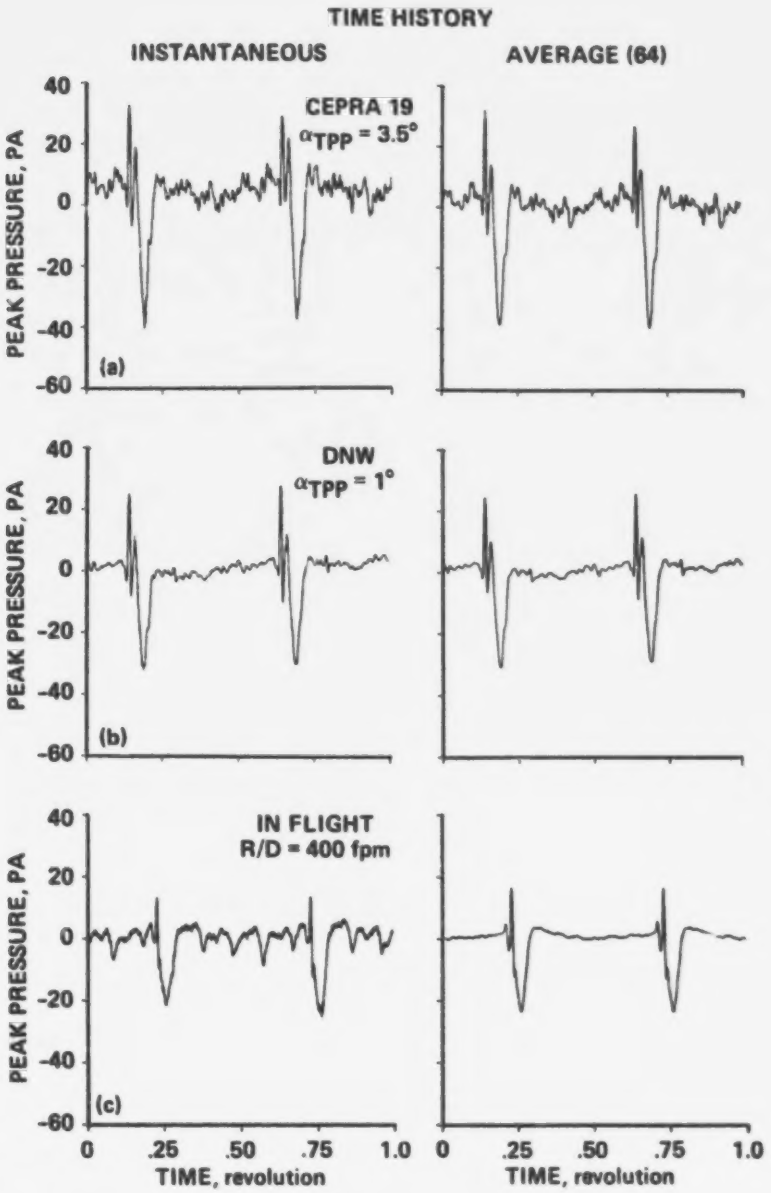

Figure 7.- Rotor acoustic comparisons, in-plane microphone: $\mu = 0.164$, $M_{AT} = 0.772$, $C_T = 0.0054$. (a) CEPRA 19 time-history, $\alpha_{TPP} = 3.5°$; (b) DNW time-history, $\alpha_{TPP} = 1.0°$; (c) full-scale time-history, R/D = 400 ft/min.

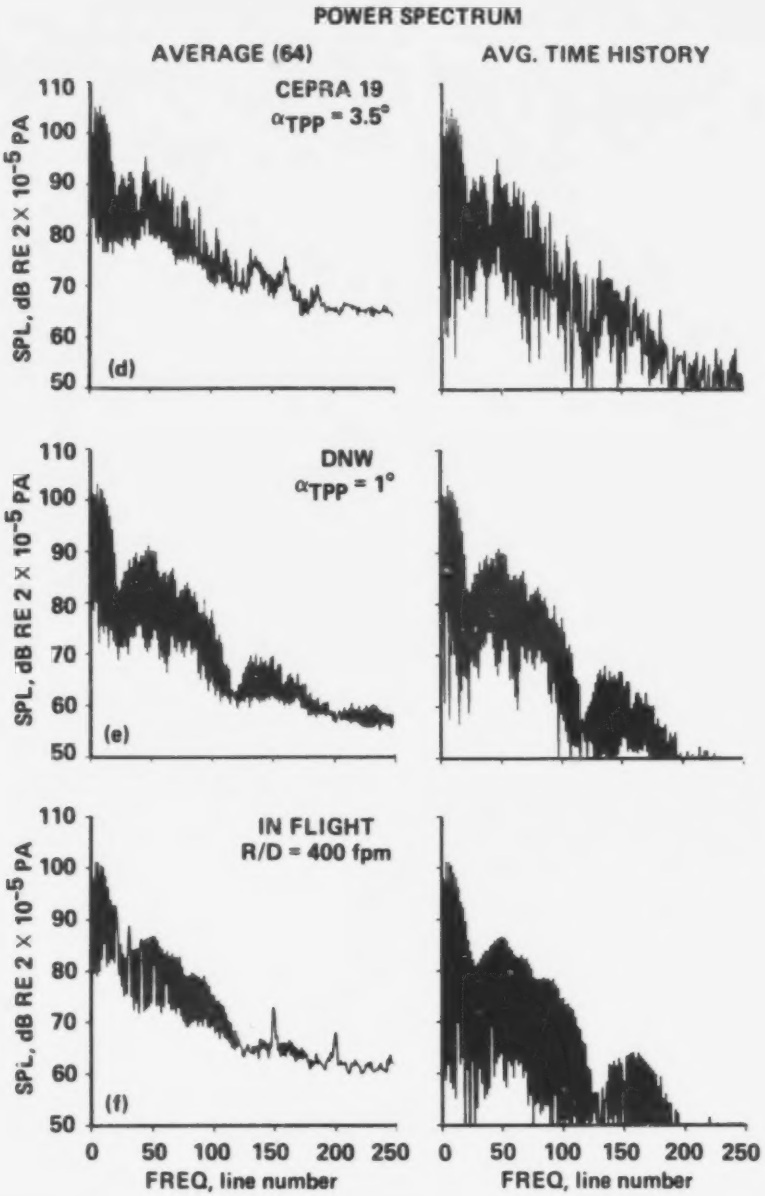

Figure 7.- Concluded. (d) CEPRA 19 power spectrum; (e) DNW power spectrum; (f) full-scale power spectrum.

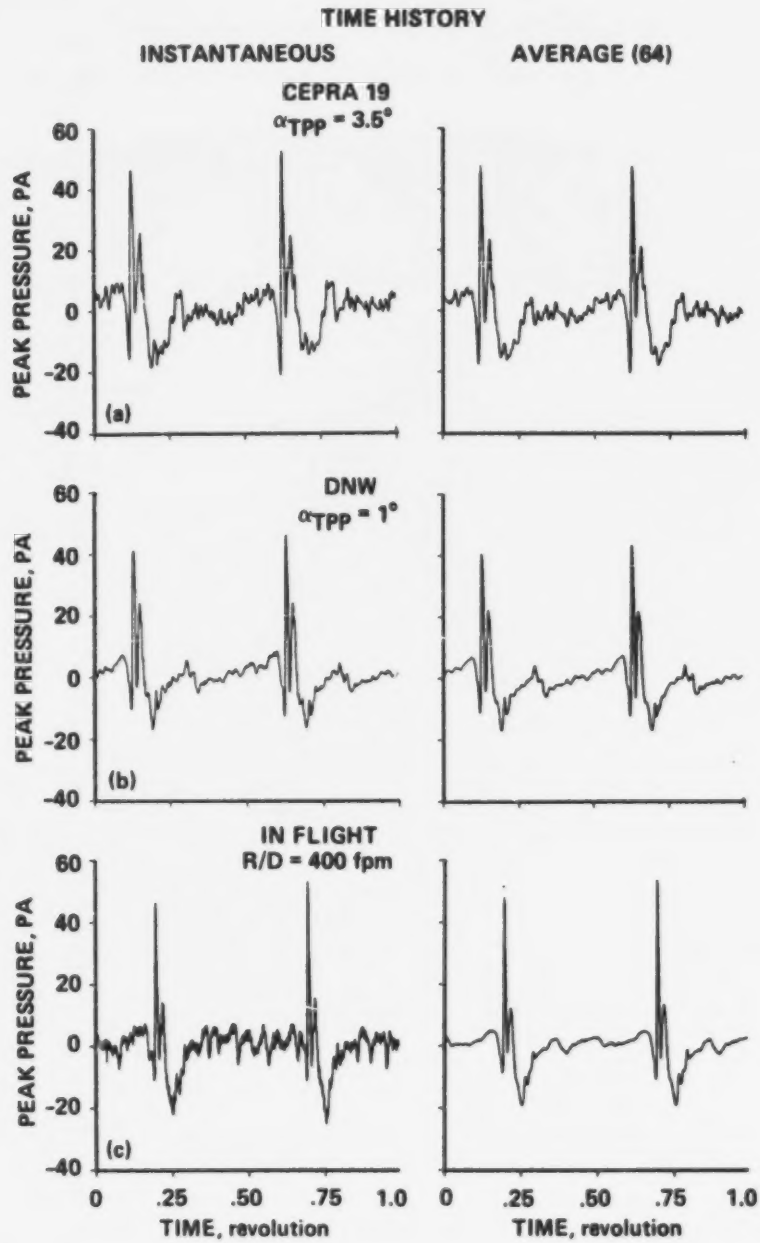

Figure 8.- Rotor acoustic comparisons, 30° below rotor-plane microphone: $\mu = 0.164$, $M_{AT} = 0.772$, $C_T = 0.0054$. (a) CEPRA 19 time-history, $\alpha_{TPP} = 3.5°$; (b) DNW time-history, $\alpha_{TPP} = 1.0°$; (c) full-scale time-history, R/D = 400 ft/min.

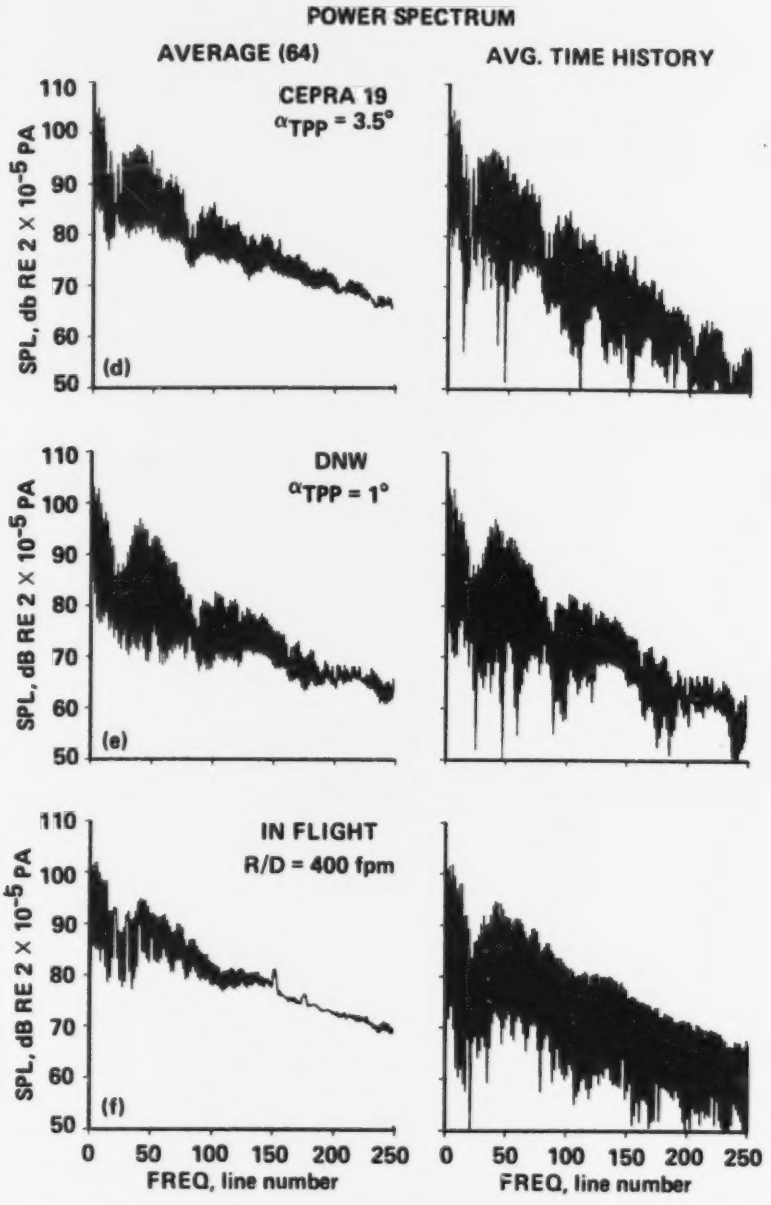

Figure 8.- Concluded. (d) CEPRA 19 power spectrum; (e) DNW power spectrum; (f) full-scale power spectrum.

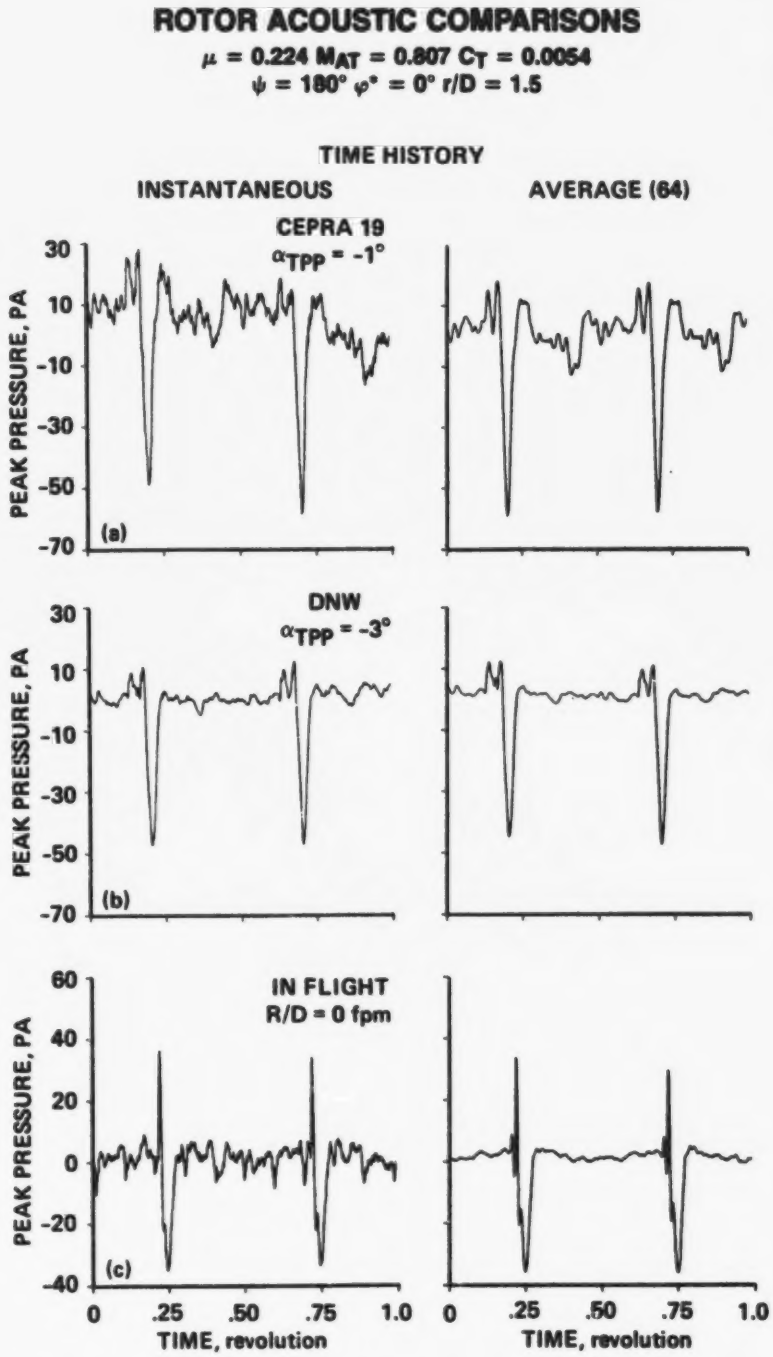

Figure 9.- Rotor acoustic comparisons, in-plane microphone: $\mu = 0.224$, $M_{AT} = 0.807$, $C_T = 0.0054$. (a) CEPRA 19 time-history, $\alpha_{TPP} = -1°$; (b) DNW time-history, $\alpha_{TPP} = -3°$; (c) full-scale time-history, R/D = 0 ft/min.

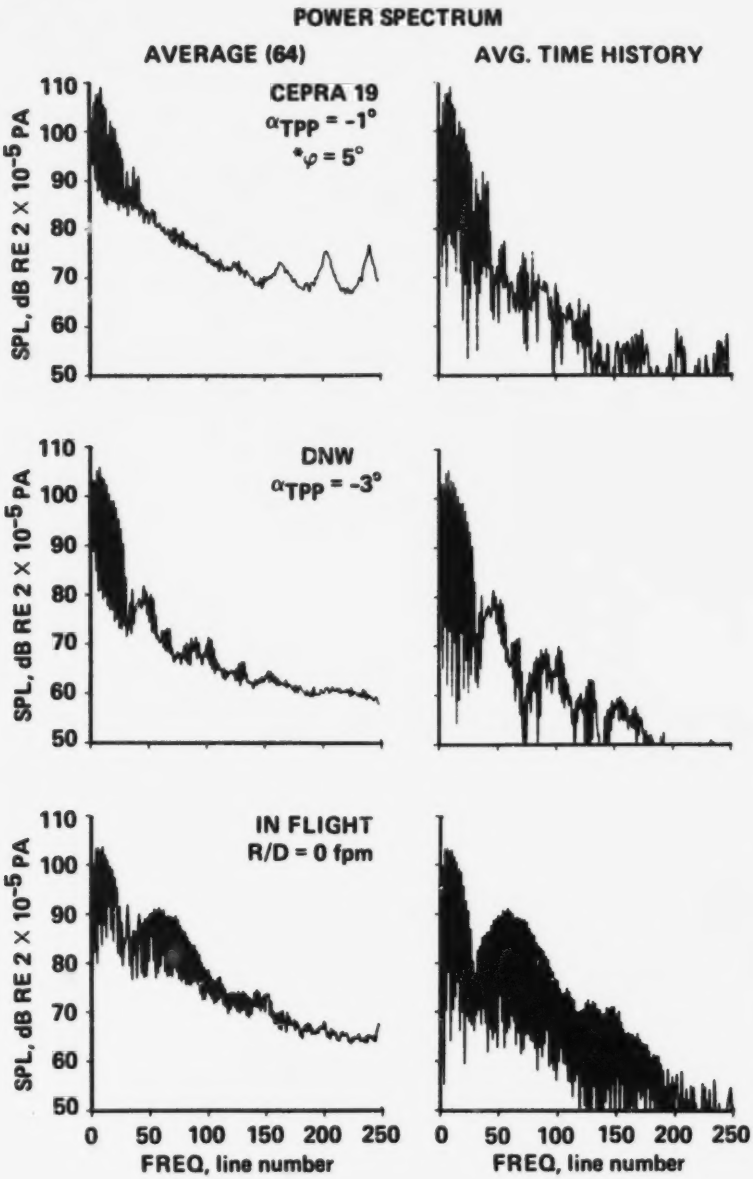

Figure 9.- Concluded. (d) CEPRA 19 power spectrum; (e) DNW power spectrum; (f) full-scale power spectrum.

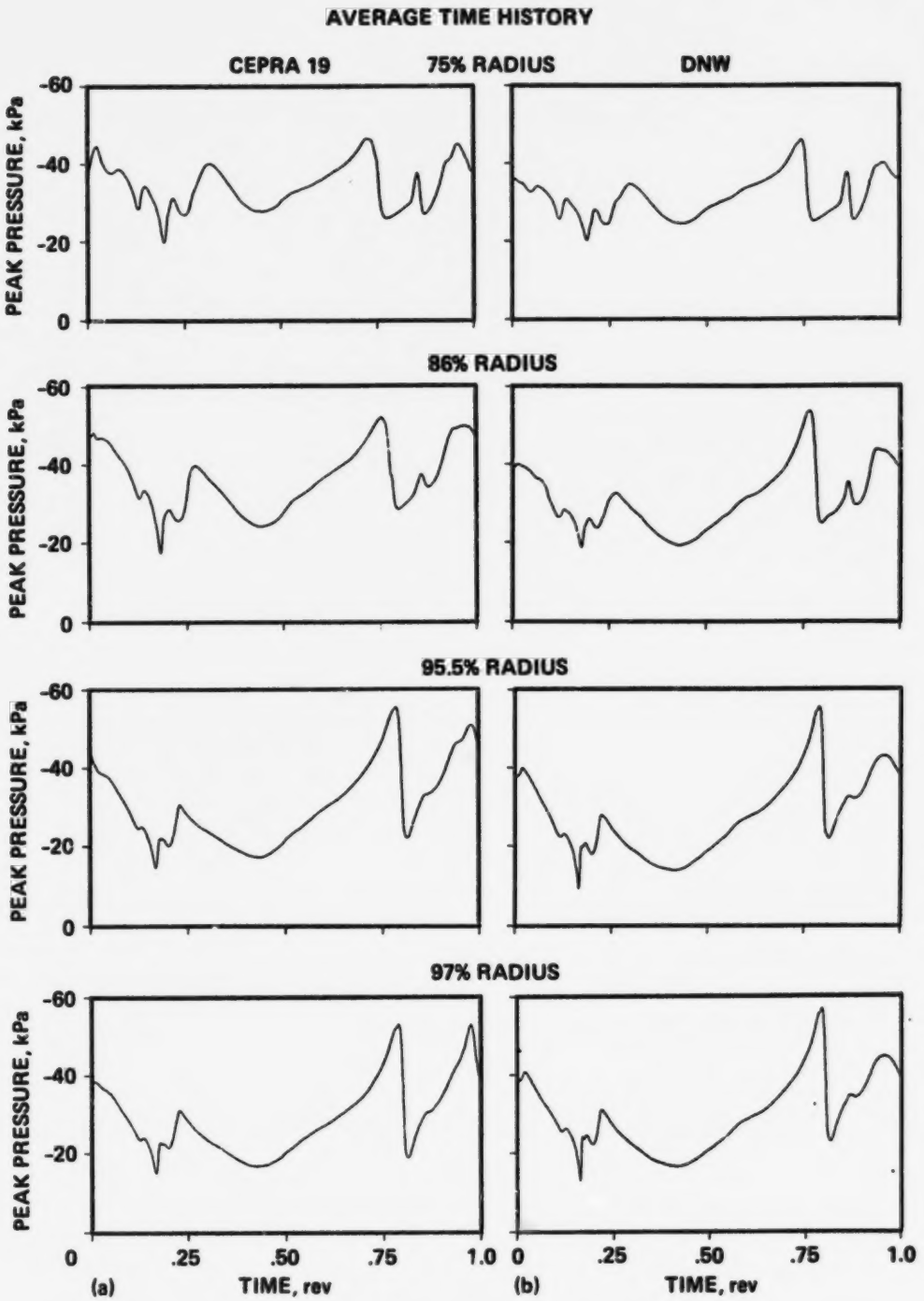

Figure 10.- Wind-tunnel comparisons of blade pressures: $\mu = 0.164$, $M_{AT} = 0.772$, $C_T = 0.0054$. (a) CEPRA 19; (b) DNW.

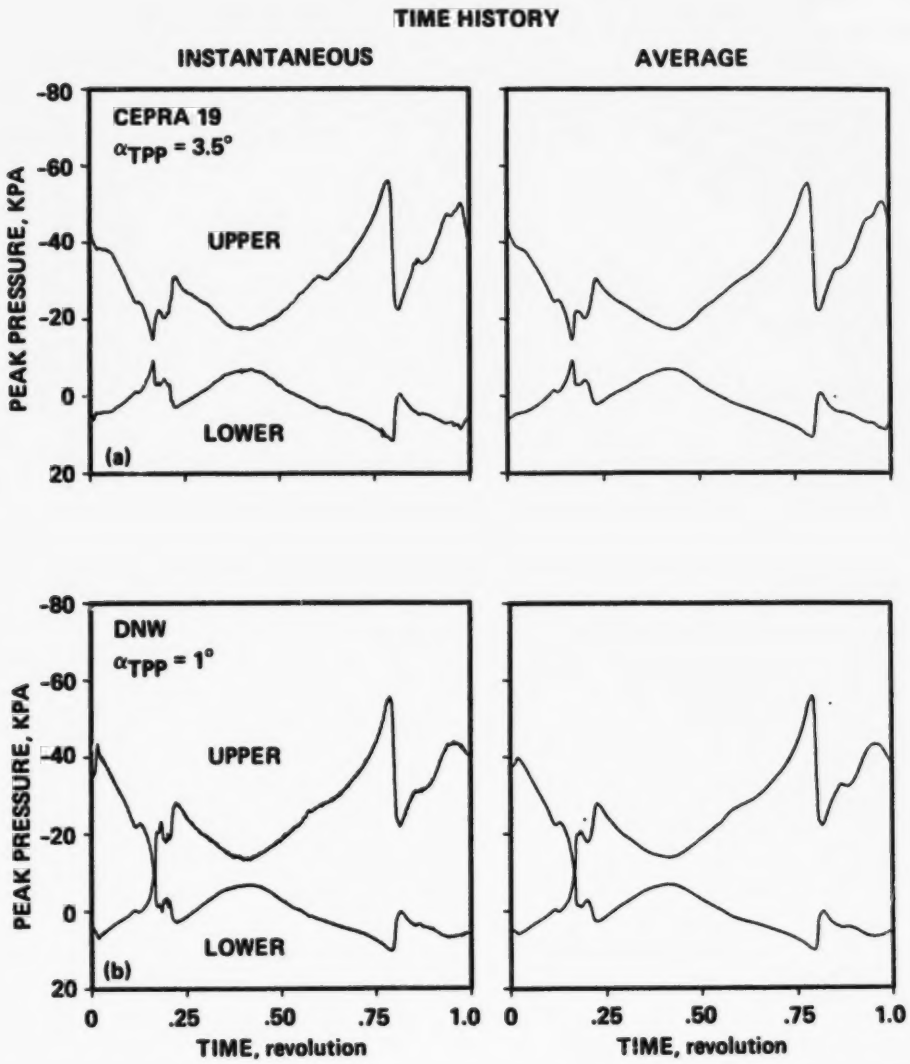

Figure 11.- Wind-tunnel comparisons of blade pressures: $\mu = 0.164$, $M_{AT} = 0.772$, $C_T = 0.0054$. (a) CEPRA 19 time-history; (b) DNW time-history.

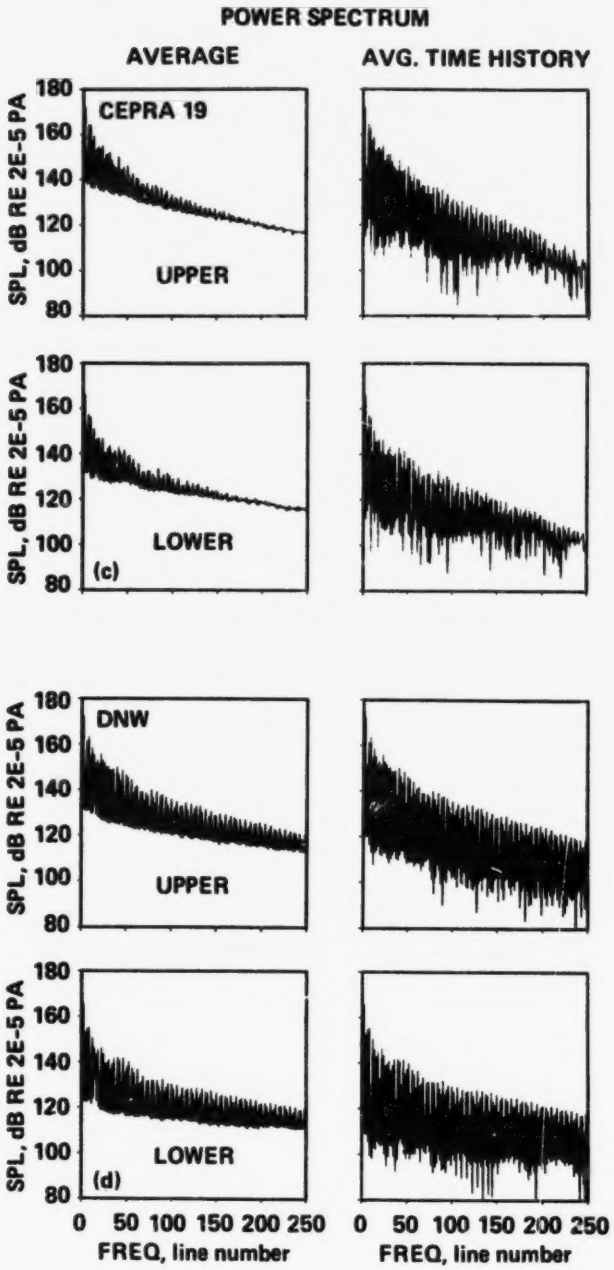

Figure 11.- Concluded. (c) CEPRA 19 power spectra; (d) DNW power spectra.

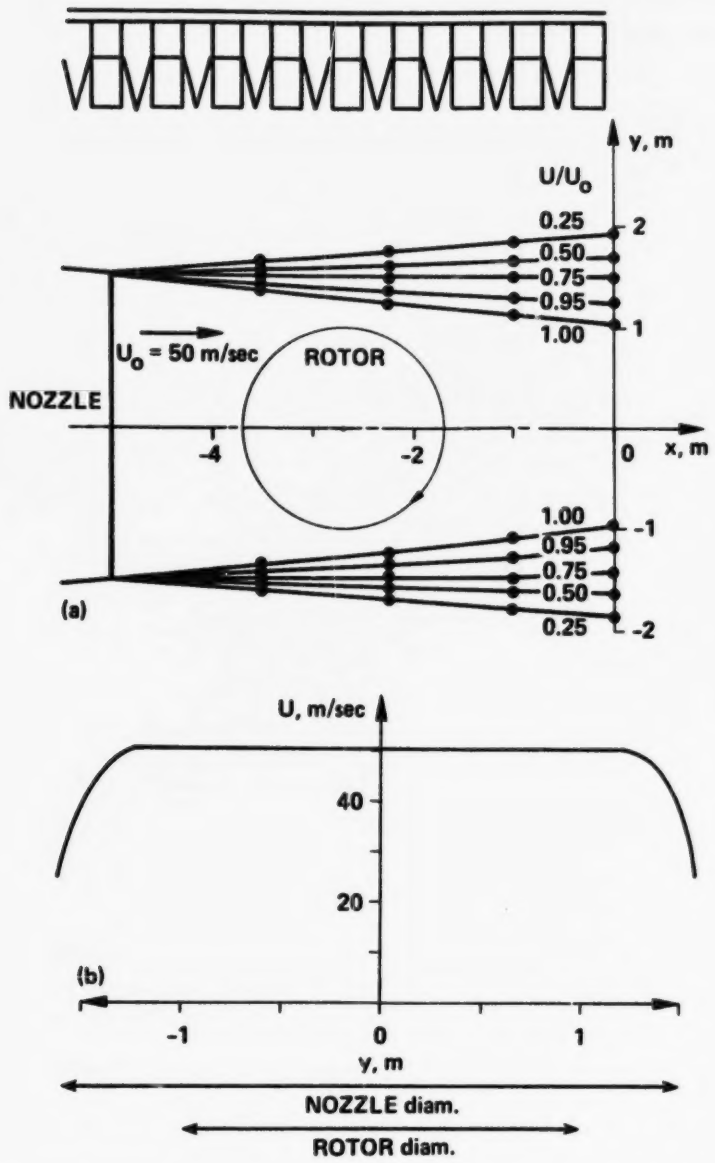

Figure 12.- Mean flow characteristics of CEPRA 19 with the 3-m nozzle at the nominal velocity U_o = 50 m/sec. (a) Top view at the height of the jet axis (z = 0); (b) axial flow profile at x = -2.677 m, z = 0 m.

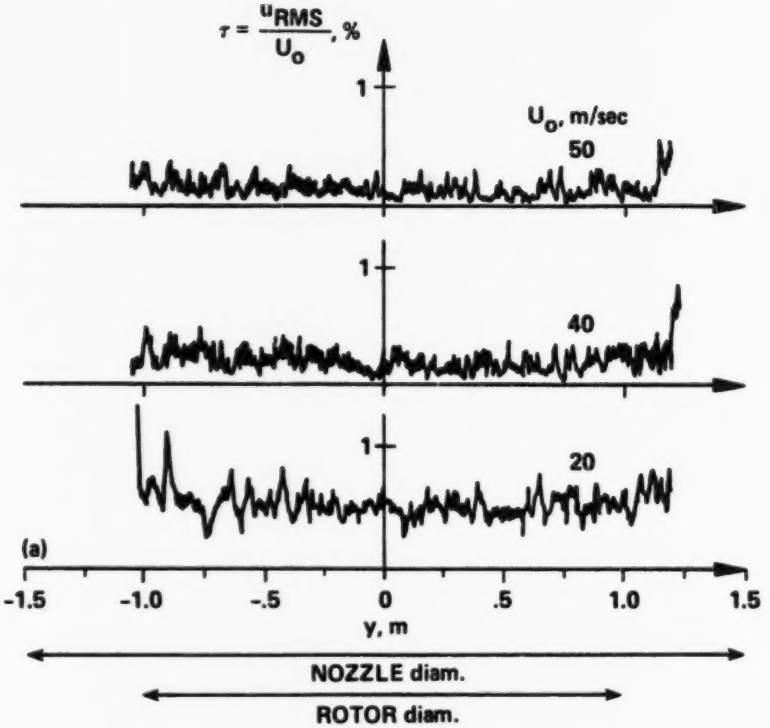

Figure 13.- Axial turbulence level across the flow at x = -2.677 m, z = -0.375 m. (a) rms value in the frequency range 0.125-2.5 Hz.

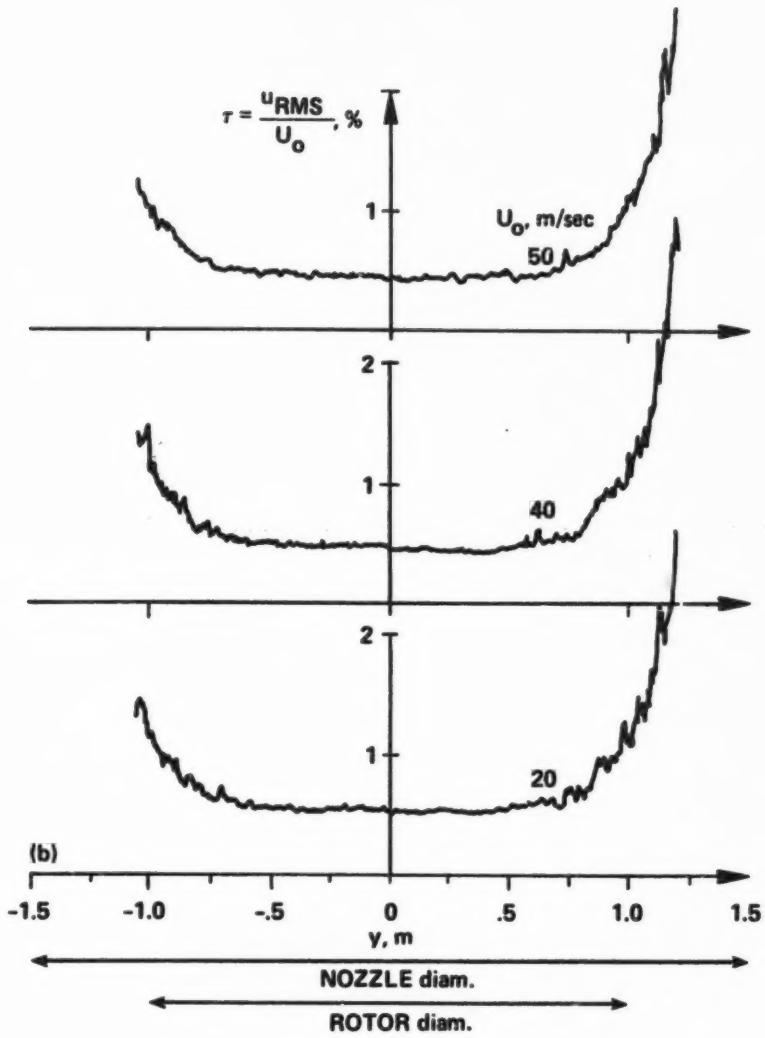

Figure 13.- Concluded. (b) rms value in the frequency range 2.5-500 Hz.

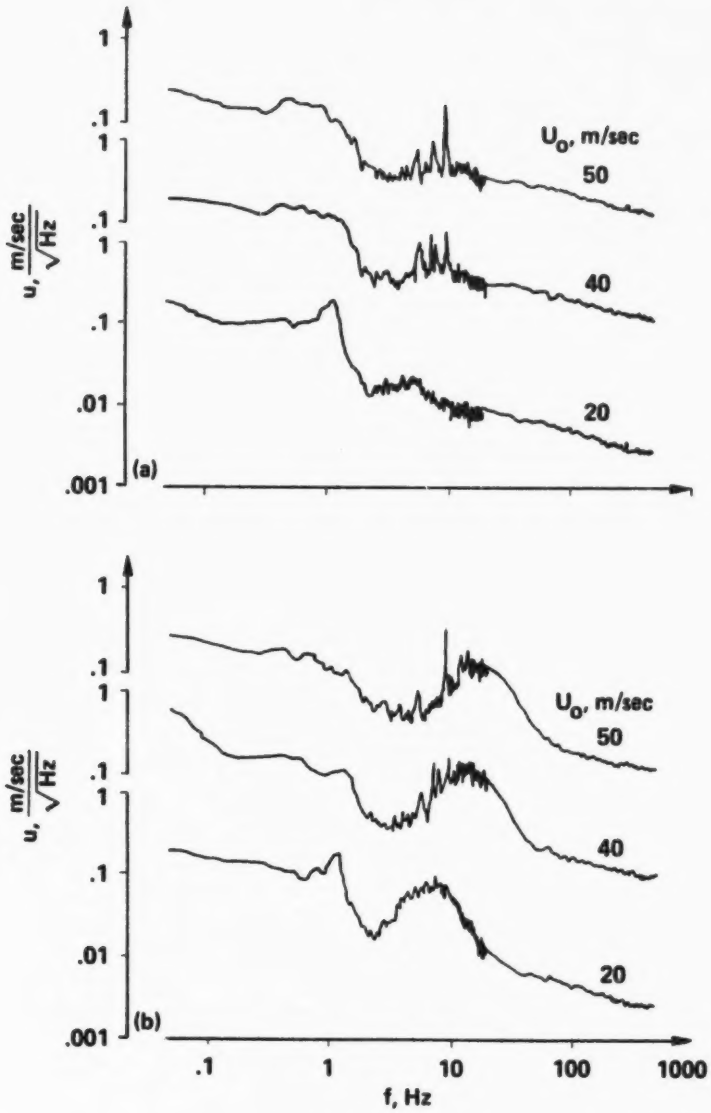

Figure 14.- PSD of axial velocity fluctuations. (a) Near the rotor hub: x = -2.677 m, z = -0.375 m, y = 0.1 m; (b) near the advancing-blade tip: x = -2.677 m, z = -0.375 m, y = 0.9 m.

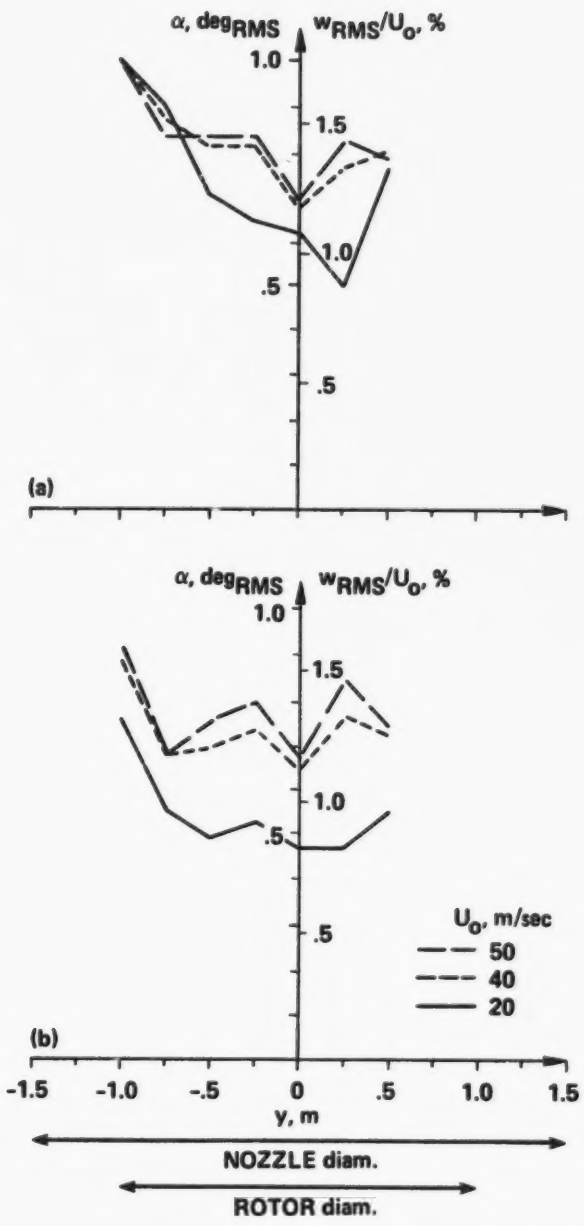

Figure 15.- Pitch-angle fluctuations across the flow at x = -2.677 m, z = -0.445 m. (a) rms value in the frequency range 0.05-20 Hz; (b) rms value in the frequency range 2.5-1,000 Hz.

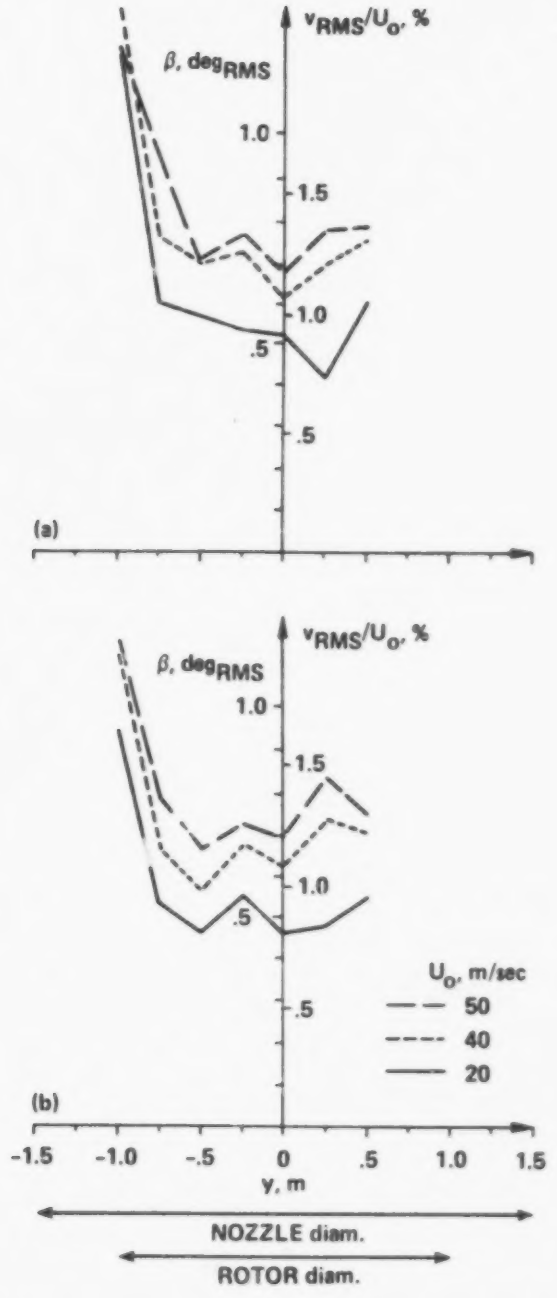

Figure 16.- Yaw-angle fluctuations across the flow at x = -2.677 m, z = -0.445 m. (a) rms value in the frequency range 0.05-20 Hz; (b) rms value in the frequency range 2.5-1,000 Hz.

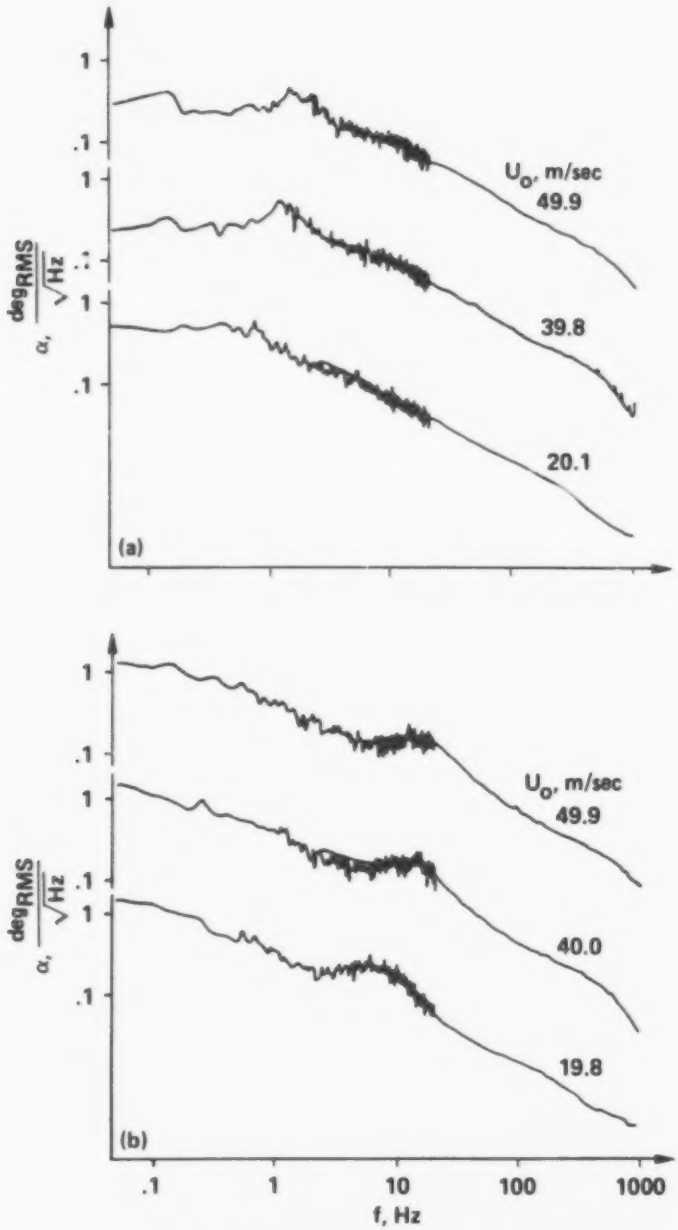

Figure 17.- PSD of pitch-angle fluctuations. (a) At the rotor hub: x = -2.677 m, z = -0.445 m, y = 0; (b) at the advancing-blade tip: x = -2.677 m, z = -0.445 m, y = -1 m.

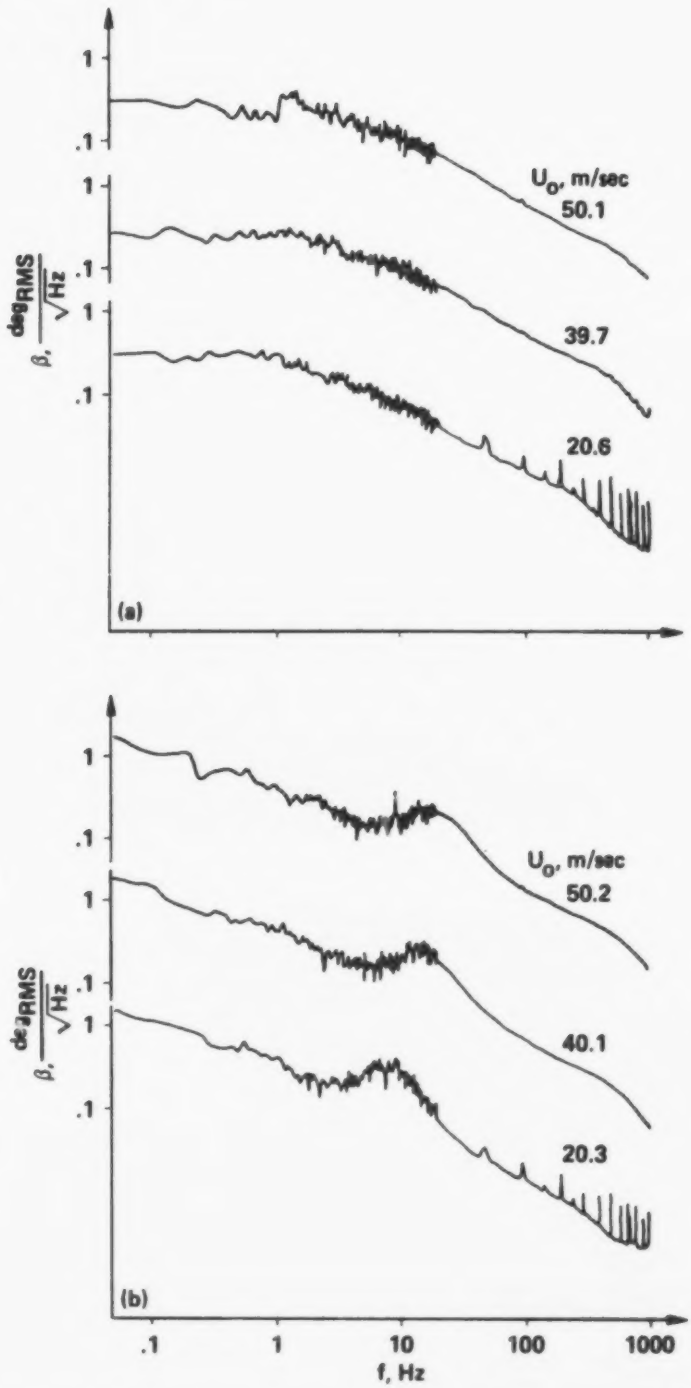

Figure 18.- PSD of yaw-angle fluctuations. (a) At the rotor hub: x = -2.677 m, z = -0.445 m, y = -1 m; (b) at the advancing-blade tip: x = -2.677 m, z = -0.445 m, y = -1 m.

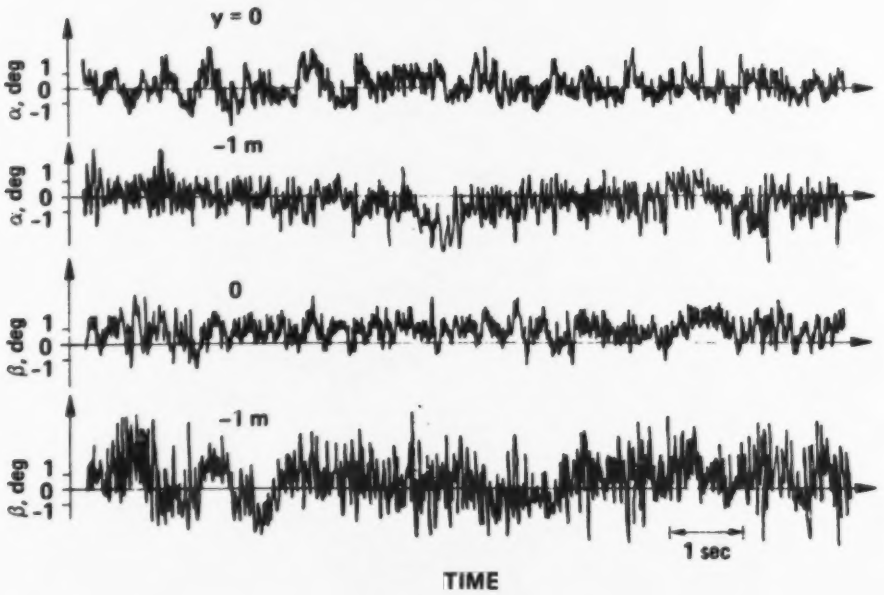

Figure 19.- Time-histories of pitch (α) and yaw (β) angle fluctuations on 10 sec at the rotor hub (y = 0) and at the advancing-blade tip (y = -1 m) locations for U_o = 40 m/sec: x = -2.677 m, z = -0.445 m (the four curves were not recorded at the same time).

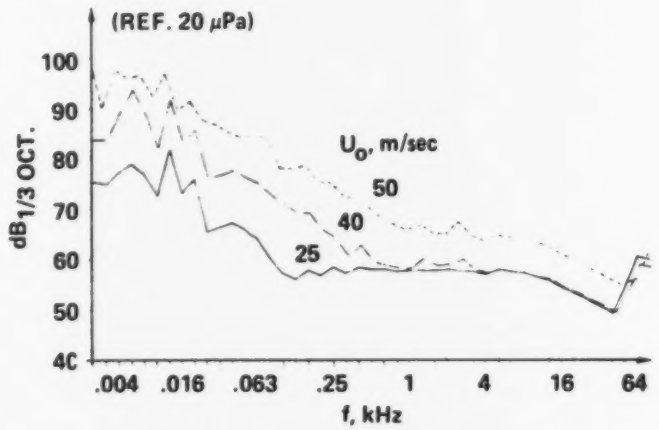

Figure 20.- Background noise at 6 m from the center of sphere (x = z = 0, y = -6 m) with the 3-m nozzle: 1/4-in. microphone without windscreen, third octave spectra.

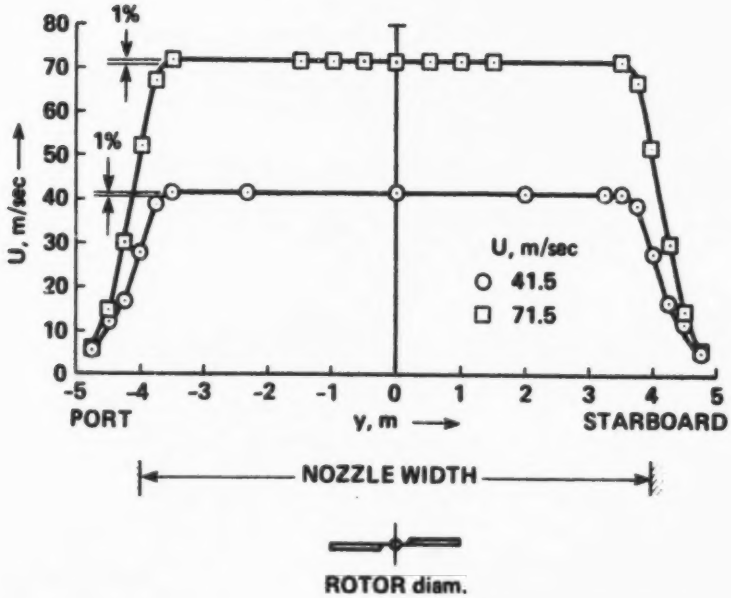

Figure 21.- Lateral mean velocity distribution at the model rotor-hub position: x = 7 m downstream, z = 0 on free-jet centerline.

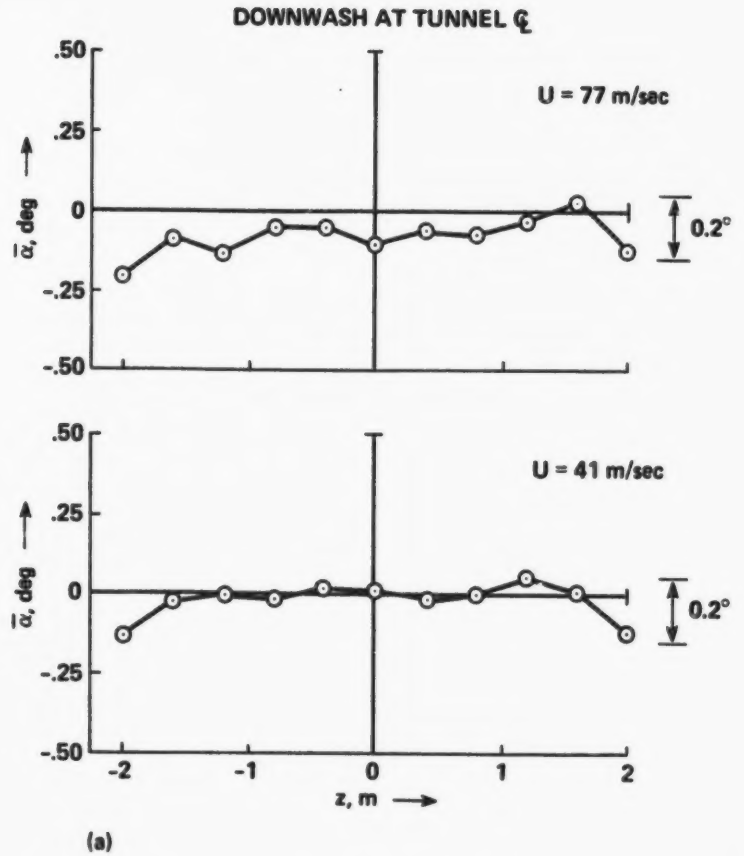

Figure 22.- Mean flow characteristics at the model rotor-hub position in the vertical plane of symmetry of the free jet on centerline: x = 7 m downstream. (a) Angle of incidence.

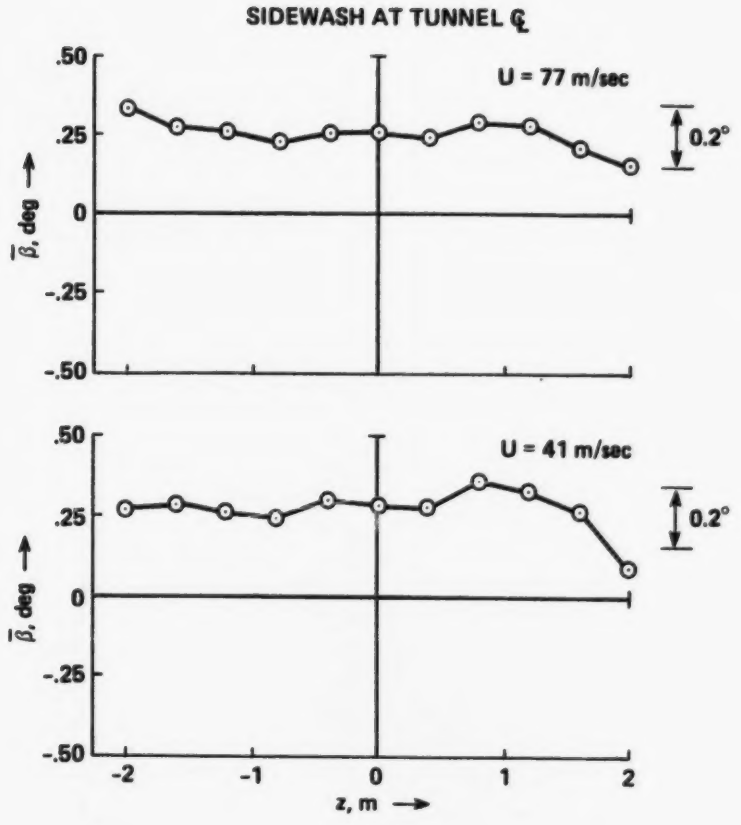

(b)

Figure 22.- Concluded. (b) angle of yaw.

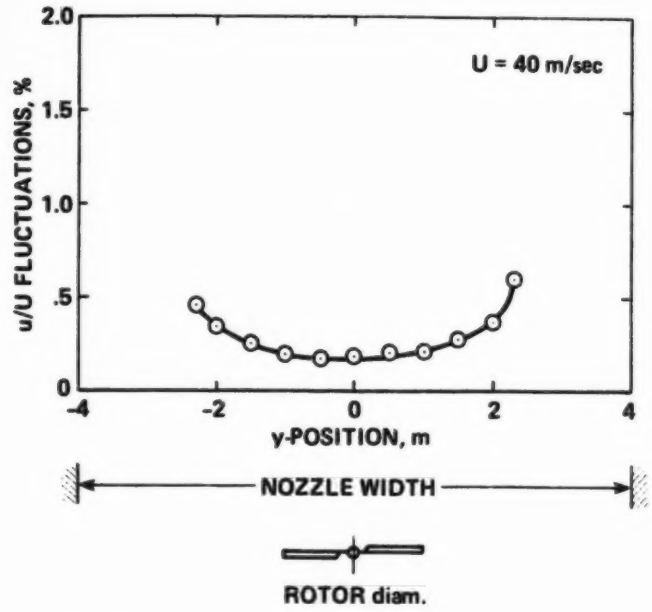

Figure 23.- Longitudinal rms turbulence intensity versus lateral position at rotor-hub position: x = 7 m, z = 0 m.

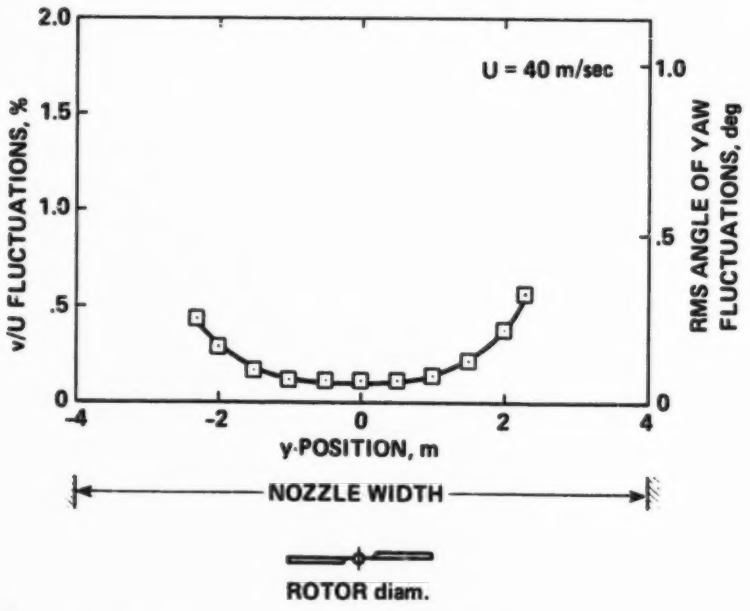

Figure 24.- Lateral rms turbulence intensity versus lateral position at rotor-hub position: x = 7 m, z = 0 m.

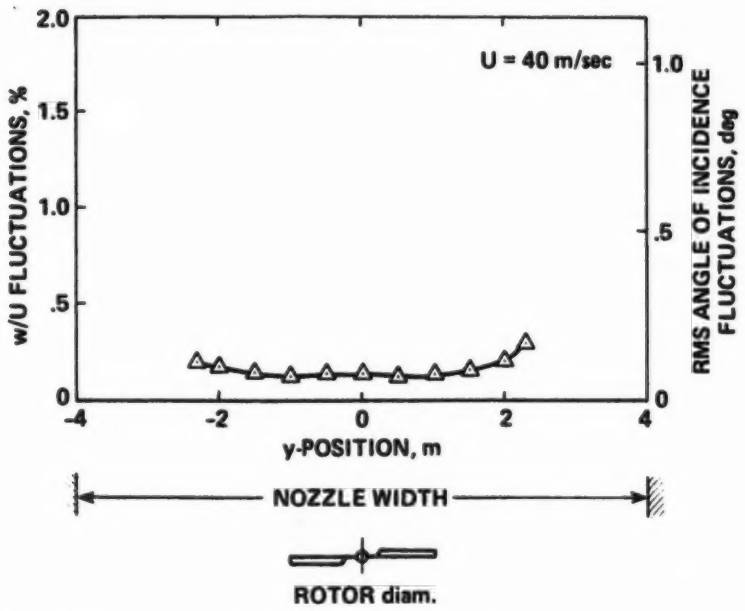

Figure 25.- Vertical rms turbulence intensity versus lateral position at rotor-hub location: x = 7 m, z = 0 m.

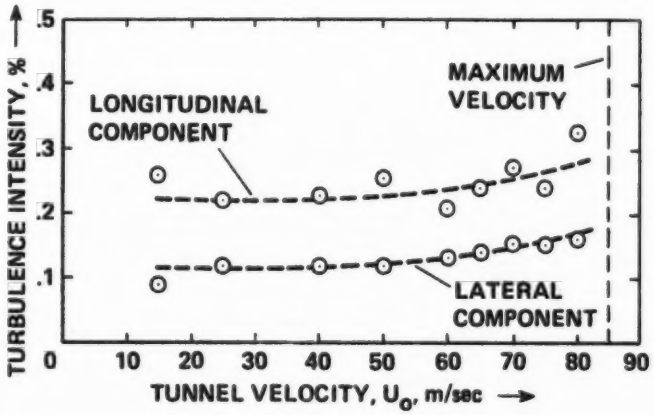

Figure 26.- Turbulence levels at the model center of the open 6- by 8-m test section versus tunnel velocity.

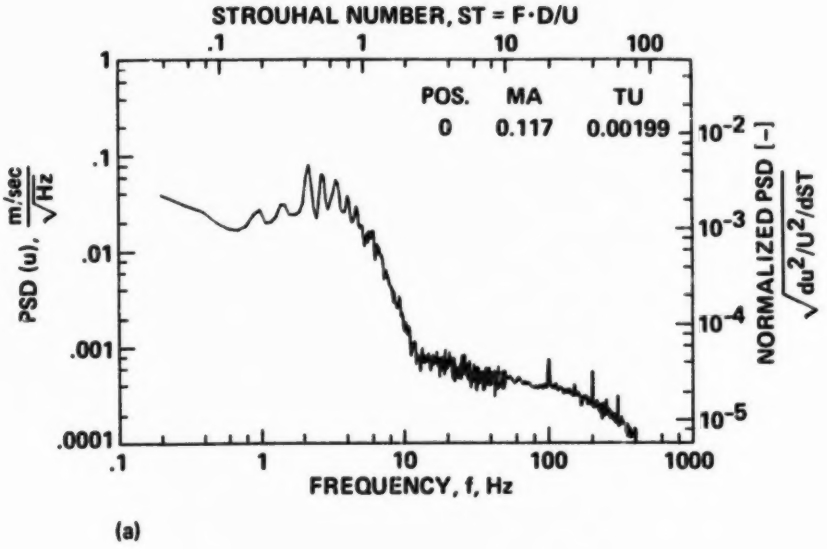

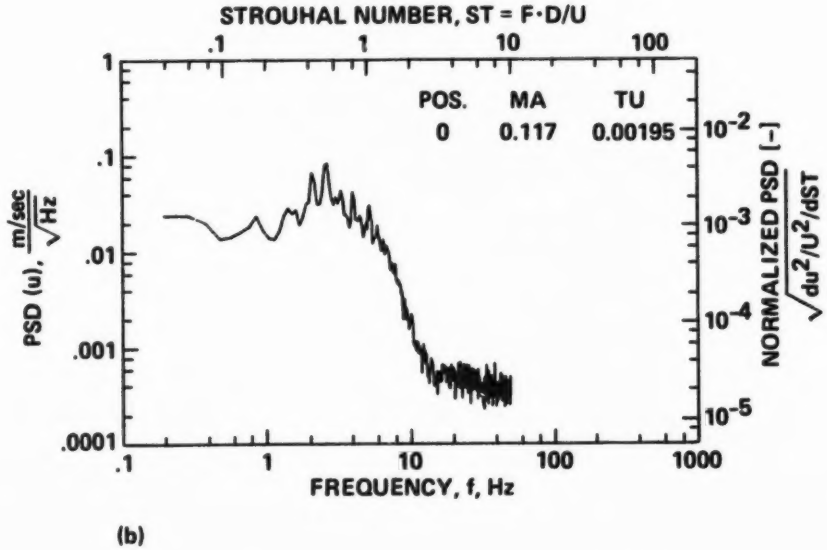

Figure 27.- PSD of axial velocity fluctuations at 40 m/sec. (a) At rotor-hub position: x = 7 m, y = z = 0 m; (b) at advancing-blade tip: x = 7 m, y = -1 m, z = 0 m.

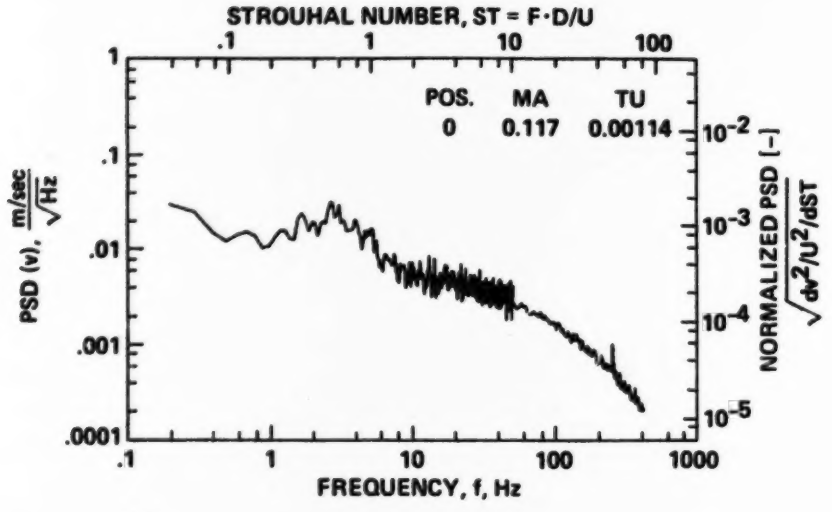

Figure 28.- PSD of lateral velocity fluctuations at 40 m/sec. (a) At rotor-hub position: x = 7 m, y = z = 0 m; (b) at advancing-blade tip: x = 7 m, y = -1 m, z = 0 m.

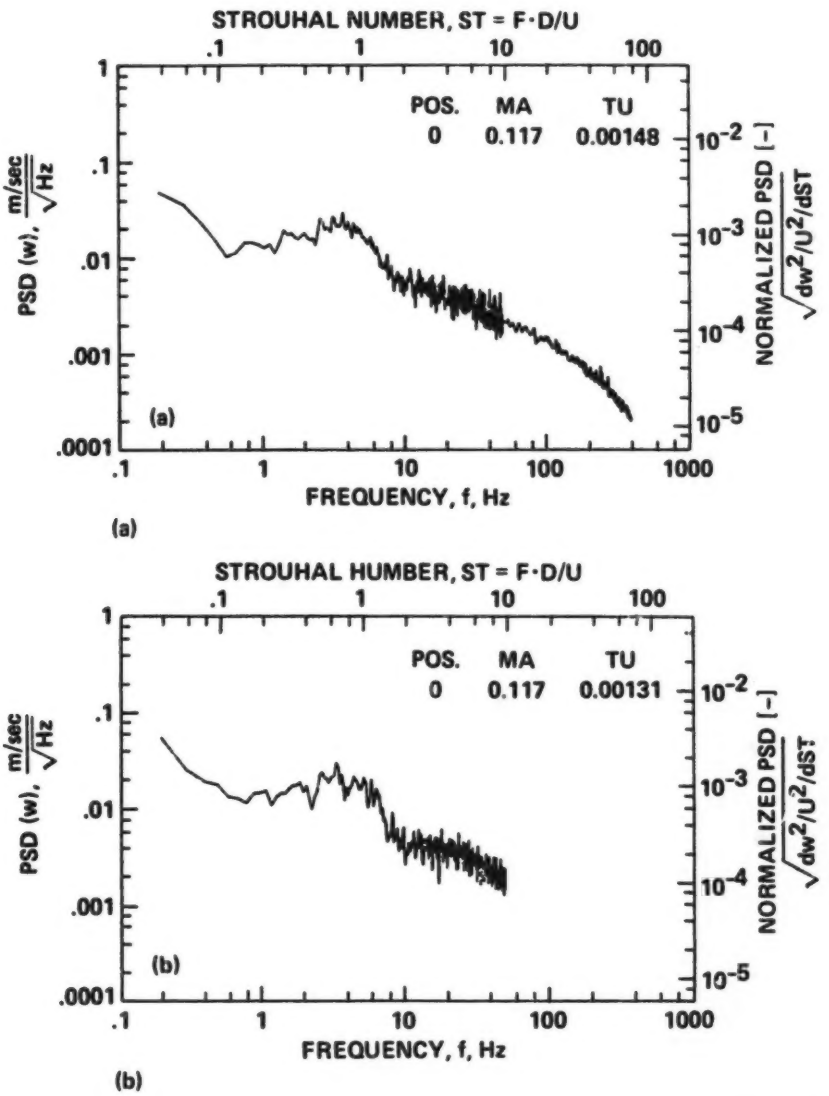

Figure 29.- PSD of vertical velocity fluctuations at 40 m/sec. (a) At rotor-hub position: x = 7 m, y = z = 0 m; (b) at advancing-blade tip: x = 7 m, y = -1 m, z = 0 m.

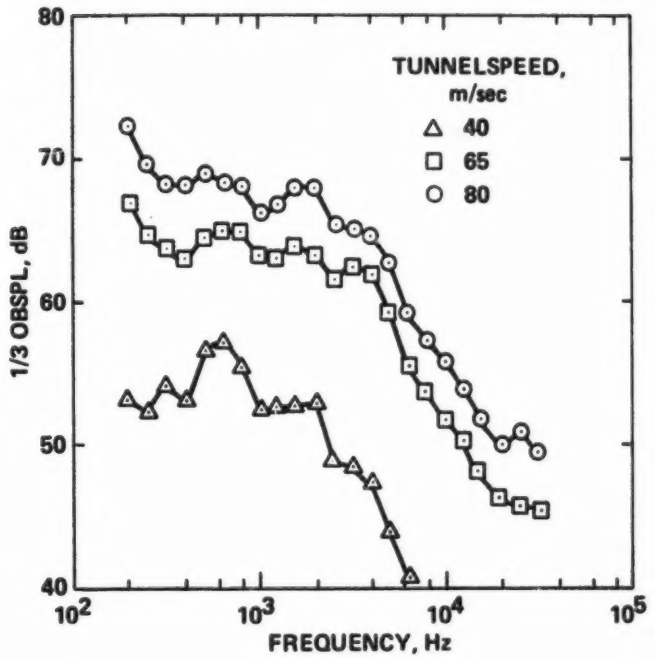

Figure 30.- Out-of-flow (12.2-m sideline) measured background noise at different tunnel speeds.

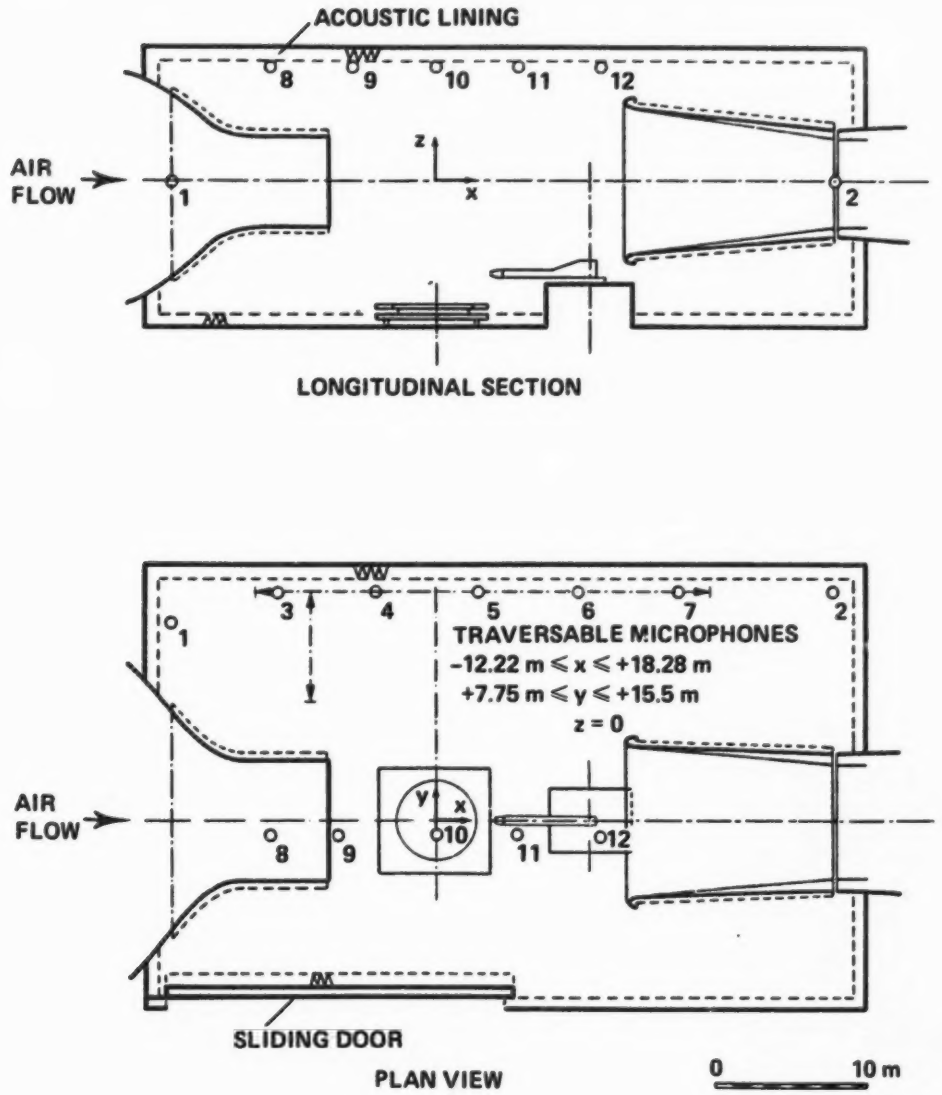

Figure 31.- Open-test-section configuration showing microphone positions during clean-tunnel calibrations.

1. Report No.	2. Government Accession No.	3. Recipient's Catalog No.
NASA TM 88364		

4. Title and Subtitle	5. Report Date
A COMPARISON OF THE ACOUSTIC AND AERODYNAMIC MEASUREMENTS OF A MODEL ROTOR TESTED IN TWO ANECHOIC WIND TUNNELS	November 1986
	6. Performing Organization Code

7. Author(s)	8. Performing Organization Report No.
D. A. Boxwell,* F. H. Schmitz,† W. R. Splettstoesser,‡ K. J. Schultz,‡ S. Lewy,§ and M. Caplot§	A-86417
	10. Work Unit No.

9. Performing Organization Name and Address	11. Contract or Grant No.
*Aeroflightdynamics Directorate, U.S. Army Aviation Research and Technology Activity Ames Research Center, Moffett Field, CA. †Ames Research Center, Moffett Field, CA. ‡DFVLR, Braunschweig, Federal Republic of Germany. §ONERA, Chatillion, France.	
	13. Type of Report and Period Covered
	Technical Memorandum

12. Sponsoring Agency Name and Address	14. Sponsoring Agency Code
National Aeronautics and Space Administration, Washington, DC 20546 and U.S. Army Aviation Systems Command, St. Louis, MO 63120	992-21-01

15. Supplementary Notes

Point of Contact: D. A. Boxwell, Aeroflightdynamics Directorate, U.S. Army Aviation Research and Technology Activity, MS 215-1, Moffett Field, CA (415)694-6167 or FTS 464-6167

16. Abstract

Two aeroacoustic facilities--the CEPRA 19 in France and the DNW in The Netherlands--are compared. The two facilities have unique acoustic characteristics that make them appropriate for acoustic testing of model-scale helicopter rotors. An identical pressure-instrumented model-scale rotor was tested in each facility and acoustic test results are compared with full-scale-rotor test results. Blade surface pressures measured in both tunnels were used to correlate nominal rotor operating conditions in each tunnel, and also used to assess the steadiness of the rotor in each tunnel's flow. In-the-flow rotor acoustic signatures at moderate forward speeds (35-50 m/sec) are presented for each facility and discussed in relation to the differences in tunnel geometries and aeroacoustic characteristics. Both reports are presented in appendices to this paper.

17. Key Words (Suggested by Author(s))	18. Distribution Statement
Acoustics Anechoic wind tunnels Model helicopter rotors Blade pressures	Unclassified - Unlimited Subject Category: 02

19. Security Classif. (of this report)	20. Security Classif. (of this page)	21. No. of Pages	22. Price*
Unclassified	Unclassified	55	A03

*For sale by the National Technical Information Service, Springfield, Virginia 22161